

QUANTITATIVE COMPARISON OF LIDAR DATA AND USER-GENERATED THREE-DIMENSIONAL
BUILDING MODELS FROM GOOGLE BUILDING MAKER

Yang Liu

Thesis Prepared for the Degree of

MASTER OF SCIENCE

UNIVERSITY OF NORTH TEXAS

August 2012

APPROVED:

Pinliang Dong, Major Professor
Murray Rice, Committee Member
Chetan Tiwari, Committee Member
Paul Hudak, Chair of the Department of
Geography
Mark Wardell, Dean of the Toulouse
Graduate School

Liu, Yang. Quantitative Comparison of LiDAR Data and User-Generated Three-Dimensional Building Models from Google Building Maker. Master of Science (Applied Geography), August 2012, 71 pp., 5 tables, 23 illustrations, references, 64 titles.

Volunteered geographic information (VGI) has received increased attention as a new paradigm for geographic information production, while light detection and ranging (LiDAR) data is widely applied to many fields. This study quantitatively compares LiDAR data and user-generated 3D building models created using Google Building Maker, and investigate the potential applications of the quantitative measures in support of rapid disaster damage assessment. User-generated 3D building models from Google Building Maker are compared with LiDAR-derived building models using 3D shape signatures. Eighteen 3D building models are created in Fremont, California using the Google Building Maker, and six shape functions (distance, angle, area, volume, slope, and aspect) are applied to the 18 LiDAR-derived building models and user-generated ones. A special case regarding the comparison between LiDAR data and building models with indented walls is also discussed. Based on the results, several conclusions are drawn, and limitations that require further study are also discussed.

Copyright 2012

by

Yang Liu

ACKNOWLEDGEMENTS

I wish to thank my major professor Dr. Pinliang Dong for his support, patience and encouragement which have greatly enhanced my graduate school experience. I would also like to thank my committee members Dr. Murray Rice and Dr. Chetan Tiwari for their comments and suggestions.

TABLE OF CONTENTS

	Page
ACKNOWLEDGEMENTS.....	iii
LIST OF TABLES.....	v
LIST OF FIGURES.....	vi
Chapters	
1. INTRODUCTION.....	1
Why Create Three Dimensional (3D) Building Models?	1
Why Develop Volunteered Information System (VGI)?.....	2
Characteristics of VGI.....	3
Application of VGI	4
Research Questions	6
2. RESEARCH BACKGROUND.....	7
A Brief Review of 3D Building Extraction from High-Resolution Images and LiDAR Data	7
Developing 3D VGI Modeling.....	12
Quality of VGI.....	13
3. STUDY AREA, DATA, SOFTWARE, AND BASIC KNOWLEDGE.....	18
Study Area.....	18
Data.....	21
Software and Tools	21
Basic Terms Related to Data and Software	22

4.	METHODOLOGY	24
	Collecting of 3D VGI Models	24
	Extracting LiDAR nDSM	28
	Comparisons of 3D Shape Signatures	29
5.	RESULTS.....	33
	3D Shape Distribution	33
	Similarity Analysis	35
	Sensitive Measure	44
	Error Tolerance	52
	Special Case.....	55
6.	DISCUSSION AND CONCLUSION.....	58
	REFERENCES	62

LIST OF TABLES

	Page
1. Authoritative Criteria of the Quality VGI (Sabone, 2009).....	15
2. Conversion from COLLADA File to Multipatch File	28
3. Correlation Coefficients (R0) between the 3D Shape Signatures of Figure 18	44
4. Correlation Coefficients between 3D LiDAR Model and the 3D VGI Model with Different Height Changes.....	54
5. Correlation Coefficients between 3D Shape Signatures (LM1 - LiDAR Vs. Multipatch 1, and LM2 - LiDAR vs. Multipatch 2).....	57

LIST OF ILLUSTRATIONS

		Page
1.	Perceived quality evaluation and average rating visualization	17
2.	LiDAR nDSM (a and c) and Google image (b) of the study area	19
3.	Five roof types: (a) flat; (b) shed; (c) gable; (d) hip; (e) desk.....	20
4.	An example of a TIN.....	23
5.	Flowchart for generating 3D VGI models and exporting to ArcGIS environment	25
6.	Locating buildings in Google Building Maker.....	26
7.	Adding 3D geometric shapes in Google Building Maker	26
8.	Extraction of building footprints from LiDAR data	29
9.	Barycentric coordinates inside a triangle.....	30
10.	Flowchart of 3D shape signature analysis	32
11.	3D building models via Google Building Maker and displayed on Google Earth	34
12.	TIN models of LiDAR-derived buildings	34
13.	3D Multipatch models viewed in ArcScene	35
14.	3D B3 building models: (a) user-generated 3D model; (b) TIN model from LiDAR	36
15.	3D B4 building models: (a) user-generated 3D model; (b) TIN model from LiDAR	36
16.	3D B6 building models: (a) user-generated 3D model; (b) TIN model from LiDAR	36
17.	User-generated 3D model: (a) B1; (b) B2; (c) B16; (d) B18.....	37

18.	Comparison of 3D shape signatures between LiDAR-derived 3D building models and user-generated 3D building models	43
19.	3D shape distributions of six functions for 18 building models	50
20.	Standard deviation histograms of correlation coefficients for six shape functions derived from different buildings.....	51
21.	3D shape signatures of six shape functions.....	54
22.	The actual building model and the modified building model with 50% decrease in height	55
23.	Comparisons of 3D shape signatures for a building derived from LiDAR point clouds and the Google Building Maker.....	57

CHAPTER 1

INTRODUCTION

Why Create Three Dimensional (3D) Building Models?

3-Dimensional is a new level of spatial data in a “digital world” (Arslan et al., 2009). 3D modeling has been widely used in several fields such as urban planning, traffic planning, pollution management, and even disaster assessment due to its capabilities in showing real-world features and phenomena in three dimensions. For example, a 3D city can illustrate spatial relationships between buildings and districts. In 2010, Autodesk Ecotect Analysis exemplified dynamic air flow analysis based on a 3D city model. The distribution of flow pollutants from traffic is illustrated by a 3D buffer map so that individuals can determine the relationship between traffic load and pollution level. Moreover, a 3D city model can provide views of underground. Moser et al. (2010) presented a case study which used a 3D visual model to create a new subway network and set up subway stations in Salzburg, Austria. Depending on the underground views from the 3D city model, engineers can remove intersected space with building basements from usable spaces.

In addition, more and more people are moving to urban areas, while more and more man-made features, such as skyscrapers and residential communities, are being built on urban lands. The increase in urban population and complexity of infrastructure may induce heavier damage in a disaster. 3D modeling is a powerful approach for emergency management and disaster assessment. For example, 3D building models provide richer information of rooftops so that levels of building damages are able to be estimated accurately (Li et al., 2008). 3D models also allows for simulating internal structures of buildings to find escaping routes in the buildings (Kolbe, 2005).

Why Develop Volunteered Information System (VGI)?

With the emergence of neogeography (Turner, 2006) which combines Web-based cartography and GIS techniques and tools, a new GIS data production paradigm, volunteered geographic information (VGI), is developed (Goodchild, 2007a; Elmadhoun, 2010). Goodchild (2007a) defines that VGI is the concept of “citizens as sensors,” meaning that citizens can voluntarily create, collect, and disseminate geographic information. Currently popular geo-web services, such as Google Earth, Yahoo!Maps, OpenStreetMap, reveal the essence of the Web 2.0. They allow public individuals to interact with geospatial information, such as creating maps using data shared by others.

VGI improves the traditional spatial data infrastructure (SDI) which is the top-down geographic information (Gould, 2007). This means SDI is developed by governments, professional institutions, and commercial organizations. SDI only covers a

small range of application since its sources are limited, its producing is somehow expensive, and its characteristics lack real-time (Coleman and Eng, 2010). Contrary to SDI, VGI is bottom-up geographic information. It can also include free “multi-media” data like photographs and videos which cannot be obtained from traditional ways (Sabone, 2010).

Characteristics of VGI

A potential impact of VGI is to improve ordinary persons understanding our earth (Goodchild, 2007a). For example, it makes it possible for ordinary persons to determine positions by Web 2.0 or mobile devices, such as Google Maps, Google Earth, GPS devices, and even mobile phones (Turner, 2006). OpenStreetMaps (OSM) and Google’s MyMaps service are used as platforms allowing ordinary users to create, edit, and modify maps (Goodchild, 2007a and 2007b; Goodchild and Glennon, 2010; Sabone, 2009). Moreover, VGI is near-real-time. It reduces response time after disastrous events and before adequate high-resolution images are available (National Research Council, 2007). For instance, a VGI group can deal with problems more effectively than specialists because individuals in the VGI group may be from the scene of events. Besides, VGI can be widely developed because it is cost-effective. Governments will no longer need to invest on mapping (Goodchild et al., 2007). Therefore, from the characteristics of VGI, a main objective of developing VGI is to fill the gaps in existing geospatial data as well as to supplement geospatial information (Goodchild, 2007a).

Applications of VGI

After the 2010 Haiti earthquake (Turner, 2010), local information collected from OSM was employed for rescue and reconstruction. A humanitarian OpenStreetMap Team was temporarily established. This team works on the assessment and management of earthquake damage based on OpenStreetMap maps and geospatial information posted by local volunteers. The project includes three steps: (1) data collection, (2) disaster response, and (3) post- disaster assessment. In the data collection step, map data in damage regions are contributed in only six hours after the earthquake (<http://www.slideshare.net/sabman/haiti-quake-public-key>). The second step involves the use of OSM data for analyzing and responding to the disaster; for example, the OSM data provide the coordinates of landslide or buildings with different damage levels, and help routing operations. Finally, the data from OSM are used for managing people at risk.

Experts and organizations intend to collaborate with ordinary individuals. They use social networks to create spatial information. These data give details about updated and local information. Wildfires threatening Santa Barbara during the 2007-2009 periods provide more examples of VGI application (Goodchild and Glennon, 2010). For example, the Zaca Fire was quickly brought under control, and the public was informed in sufficient time to facilitate evacuation of threatened areas (Goodchild and Glennon, 2010). These exemplified social networks of VGI, such as Flickr and Youtube. Comparing

to official agencies, the social networks related with VGI provide more updated and cost-effective information (Goodchild and Glennon, 2010). Beside, Goodchild and Glennon (2008) give another example: in November 2008, another fire, Tea Fire, also ignited in Santa Barbara. VGI respond to this immediately on Web-based community. Although Tea Fire is stronger and quickly spread, it burns for only 2 days and damaged 230 architectures (Goodchild and Glennon, 2008). VGI is used by Emergency Services and Roadside Assistance (ESRI, 2011). From these emergency cases, integration of VGI Public and Participation GIS (PPGIS) brings up the needs of timely and cost-effective emergency management (Bugs et al., 2010).

Some other VGI programs are listed below. The Globe Program is an interagency program supported by NASA, NSF and US State Department. This program provides opportunity to learn more about our earth. In the program, VGI is the main source of information. It is created by Globe Alumni organization (Sabone, 2009). The program encourages people to collaborate with each other to collect and share their information on this website. In addition, the TomTom Mapshare Service (TomTom, 2007) provides a media to allow their customers to update, add, and delete maps in devices timely (Sabone, 2009). Moreover, New Jersey government collaborates with volunteers to hold mapping vernal pools, which provides a web mapping interface (Lathrop et al., 2005).

Research Questions

The purpose of this study is to quantitatively compare LiDAR data and user-generated 3D building models created using Google Building Maker. There are two major research questions:

- (1) What measures can be used to quantify the differences between LiDAR-derived 3D building models and user-generated 3D building models created using Google Building Maker?
- (2) What are the potential applications of the quantitative measures in support of disaster damage assessment such as post-earthquake damage assessment?

CHAPTER 2

RESEARCH BACKGROUND

A Brief Review of 3D Building Extraction From High-Resolution Images And Lidar Data

Traditionally, 3D building models can be built from two remote sensing data sources: (1) image data (Pollefeys et al., 2008), and (2) light detection and ranging (LiDAR) data (Früh and Zakhor, 2004; Charalambos Poullis and Neumann, 2008). 3D models demonstrating urban structures can be automatically extracted from aerial imagery (Haala and Hahn, 1995). In the early 1990s, the first scanning airborne lasers (ALS) are introduced for data collection (Stephan et al., 2010). Li et al. (2008) proposed an approach that detects degrees of damages after earthquake by comparing pre-earthquake and post-earthquake 3D building models. An automated approach assessing building damage after an earthquake is developed by deriving 3D shape signatures of buildings from LiDAR data (Dong and Guo, 2011).

High-resolution Images and LiDAR data have been considered as the top priorities for building extraction (Wei et al., 2004; Zhou et al., 2004). High-resolution images are typical sources developed by remote sensing techniques for building extraction, which provide shadows cast by buildings so that operators could make analysis of 3D building models (Xiao et al., 2004). It is useful to get shadow information for verifying whether a feature exists as well as for identifying boundaries of buildings. Also, depending on shadow of buildings shown in aerial images, it is possible to measure heights of buildings (Huertas and Nevatia, 1988). Additionally, high resolution images make it possible to display textures of 3D building models (Frueh et al., 2004). Textures mapping of 3D building models provides a lot of details of roof types and information of vertical walls. In recent years, high-resolution images are used for extracting 3D geometric models of buildings (Huertas and Nevatia, 1988; Sahar and Krupnlk, 1999; Kolbe et al., 2000).

Earthquake damage can be assessed with both high resolution imagery and LiDAR data. Since LiDAR data provide elevation information of buildings, they have a crucial advantage over high resolution imagery in 3D building model extraction. In fact, not only do LiDAR data provide points with height values to create digital surface models (DSMs) (Zhou et al., 2004), but also they are used to construct Triangulated Irregular Networks (TIN) by filtering LiDAR data points (Tse et al., 2004). A high density of LiDAR data points leads to high quality and accuracy of building detection (Alexander et al., 2009).

A great variety of processing techniques have been developed for extracting 3D buildings from high-resolution images and LiDAR data. These techniques are generally operated by a combination of high-resolution images, LiDAR data, and GIS. A preliminary step in this process is to extract building footprints and recognize shapes. Edge detection from high-resolution images is a prevalent technique for building extractions (Sahar et al., 2010). Edge detection is based on histogram peak selection to examine features in parcels. Because there are a limited number of buildings in a parcel, a building in this parcel will be detected based on their three significant bands (Sahar et al., 2010). If the histogram peak is consistent, it represents the roofs of the building. Next, using shadow-based verification and geometry-based elimination, the areas of building footprints will be accounted in order to remove segments that do not fulfill the buildings (Sahar et al., 2010). Conversion from raster to vector is done in the GIS-based stage so that the exterior rings of buildings including convex hull of the 2D shape can be created. The research by Sahar et al. (2010) gives an automated GIS method to extract a large numbers of buildings in an area. However, the method is characterized by three limitations: (1) the images used in the study cannot be updated immediately. (Sahar et al., 2010); (2) it only can extract simple roof tops since there is no analysis of texture-based images; (3) not all of buildings can be detected because of missed significant spectral signatures (Sahar et al., 2010). Brenner et al. (2003) use multispectral images and normalized digital surface models (nDSMs) derived from a scanning laser altimeter to determine 2D building polygons. This process separates buildings from natural

features such as grasses and trees. The nDSMs are used to separate features with different elevations. The colored infrared images provide information to discriminate among buildings and trees that have same elevation (Henricson et al., 1996). If this information is available, extracting building footprints is successful in the first stage of the automated method. However, since an Imaging Laser Altimeter has to be installed on an aircraft or a satellite, this method can be expensive. Therefore, updating of building information can be difficult. Many algorithms have been applied as ancillary means for footprint extraction. Lee et al. (2003) and Wei et al. (2004) use the Hough Transform method to classify building top shapes. The Hough Transform is a technique that helps to find imperfect shapes to revise the shapes. For extracting building footprints, this technique is applied to detecting lines that can construct effective polygons (Wei et al., 2004). The Hough Transform also helps to determine the directions of buildings and extract building rings by detecting parallel lines and perpendicular lines (Lee et al., 2003). A Bayesian technique is a method of probability and statistics. This algorithm is used to compute the posterior probability of building footprints (Wang et al., 2007). They describe three steps of the algorithm: (1) locating points on the boundary lines, (2) creating cursory footprints, and (3) determining a final building footprint using posteriori probability. This method by Wang et al. (2007) is used for eliminating great amounts of noise around building boundaries and extracting accurate building footprints. Furthermore, the Bayesian technique can be applied to extracting entire 3D building models (Wang et al., 2007).

Many techniques are developed to extract 3D building models. Automated extraction of 3D models is widely completed by collaboration of remotely sensed data and GIS (Lari and Ebadi, 2004; Zhou et al., 2004). Other previous works employ a variety of approaches that are used to extract 3D buildings through from LiDAR data and digital aerial images. Bapsavias et al. (1995) completed a project, which indicates that 3D models can be accurately extracted from LiDAR data and orthoimages through three steps: edge extraction, mathematical algorithms, and height bins. Bapsavias et al. (1995) solved two main difficulties: how to avoid merging two buildings close to each other and how to separate buildings and vegetation. Moreover, Zhou et al. (2004) propose to integrate orthoimage details into LiDAR points cloud. Their method is completed to extract 3D building models based on nDSMs, digital building models (DBMs), and digital terrain model (DTM). The main contribution is to develop a method of generating high quality DBM so that accurate building roofs can be modeled. Triangulated irregular networks (TIN) from LiDAR points cloud are considered as basic models to identify different types of building roofs so that 3D building models can be accurately extracted (Alexander et al., 2009). This method is limited by densities of LiDAR points. In fact, if the high-resolution LiDAR data are available, extraction will be more accurate. Also, patched roof slopes influence the accuracy of 3D models. Normally, flat building roofs are extracted easily.

Developing 3D VGI Modeling

Since traditional data collection is often expensive, and existing methods for creating 3D object models are very complex (Benner et al., 2005), the emergence of VGI provides a new paradigm for geospatial data collection, including 3D geospatial data collection. For example, many virtual globe programs, such as Google Earth and Bing Maps 3D, allow public interaction with 3D geographic information by easy and free (Jones, et al., 2010). Moreover, the application of online tools, such as Google Building Maker and Google SketchUp, promotes 3D VGI modeling (Schilling et al., 2009). OpenStreetMap is a good example which helps generating 3D-city models by volunteers (Neubauer, et al., 2009). Schilling et al. (2009) show GIS services and 3D city models coming together for storing and analyzing rich 3D city models. Two examples of OSM for 3D visualization are KOSMOS Worldflier (<http://igorbreic.net/category/3d>) and the OSM-3D projects (<http://www.osm-3d.org>) (Geotz and Zipf, 2011). The German government considers that 3D VGI data contribute the most important portion of information of city planning (Over et al., 2010). Although, most 3D VGI is somehow difficult to completely fulfill the accuracy, which they need to be evaluated by official services, it still reveals its huge advantages of collecting vector data of objects for 3D models.

Quality of VGI

Current technologies mainly focus on enhancing generation and dissemination of VGI. However, since VGI techniques are related to amateurs who produce and disseminate the geospatial information, the quality of VGI is a main concern before VGI can be used. There are several questionable factors raising this concern: Where do the VGI data come from (Coleman, D. J. & Eng. P., 2010)? Who generates the VGI (Coleman, et al., 2010)? What are the objectives of the individual contributors (Gould, 2007)? These three questions are related to VGI sources. Whether the sources of VGI are credible influences the quality of VGI (Flanagin & Metzger, 2008). For example, OpenStreetMap depends on GPS data collected by different individuals to maintain its huge information structures to be latest and comprehensive. The multiplicity of data sources makes it complex to verify the credibility of VGI (Flanagin & Metzger, 2008). In addition, the quantity of data controls the credibility of user-generated information (Rieh & Danelson, 2007). Plentiful data allows users to compare the data from different individuals so as to obtain suitable data. Likewise, tools that individuals use to produce VGI impact the credibility of VGI (Sabone, 2009). Different tools have different errors standards. Depending on different applications of VGI, individuals should use different tools. For example, some of the techniques of positions are suitable for outdoor areas and broad range coverage (Sabone, 2009). Like GPS, it is to position through receiving signals from four satellites and obtains latitude and longitude (Barnes, 2003). While GPS can provide high accurate position points, some positioning techniques have relatively

low accuracy. For instance, Cell of Origin (COO) detects points with distances from 500 m to 15 km (D'Roza & Bilchev, 2003). Consequently, the point positions in OpenStreetMap have different levels of accuracy because they may be collected by different position devices.

Although there is total difference between the top-down data (data obtained from professional organizations and then used in sub-system) (Gould, 2007) and bottom-top data (data are created by users; and then many of them are used by both users and professional organizations) (Bishr & Kuhn, 2006), the complementation of these two improves the quality of VGI (Gould, 2007a). Authoritative datasets are selected as references for filtering errors and inaccuracies of user-generated data. For example, Sabone (2009) suggests several criteria from Canadian Geographic Data Infrastructures (CGDI), which are National Road Network (NRN), National Topologic Database (NTDB), and CanVec, as standards and specifications of data accuracy. Table 1 summarizes these authoritative criteria are used for examining whether the VGI is complete and accurate, and the table gives explanation about these criteria respectively. Among the criteria, positional accuracies of VGI are influenced by Location Based Services (LBS) devices which include spatial positioning techniques, mobile communication infrastructure, wireless Internet, and Web-GIS. Because of different applications and purposes, the positional accuracy requirements of VGI are different (Barnes, 2003). For example, GPS/A-GPS provides relatively high accurate geo-spatial data for emergency services and roadside assistance. Other applications, such as traffic

calming, vehicle navigation, and asset tracking, need to track or navigate using other devices like EOTD (Enhanced Observed Time Difference)/COO (Cell of Origin) having a larger range of accuracy.

Table 1. Authoritative Criteria of the Quality VGI. (Sabone, 2009)

Elements of VGI	Authoritative databases	Description
Data Structure	NRN and NTDB	There must be a complete VGI structure consisting of geometric description (e.g. line, points, or polygon), descriptive representation (e.g. coordinate system), identifier (e.g. names of roads or POI), and metadata.
Metadata	NRN	The metadata of VGI minimally includes source (e.g. GPS) and accuracy of the information.
Positional accuracy	NTDB, Can Vec, and NRN	VGI must meet a planimetric accuracy criterion.
Attribute accuracy	CGDI	VGI should include names and types of features (e.g. E I-35 highway).
Uncertainty	Errors of attributes: NRN and Can Vec; Errors of positions: Traditional mapping specifications	Errors of attributes should not be more than 5%; Errors of positions should not be more than 10%.

Evaluating quality of 3D VGI models is more complex than evaluating 2D VGI quality. Currently, 3D VGI mostly focuses on applications of visualization. For example, OpenStreetMap provides more information of city regions and building geometries (Neubauer et al, 2008). It allows public to capture points of interest, land uses and even structures on the earth surface. Besides, integration of data from OpenStreetMap and

Shuttle Radar Topography Mission (SRTM) attains DEMs simulating building geometries. Many user-created 3D models are obtained from Google Earth (Jones, 2011). However, there is less quality information to persuade users to completely trust these 3D VGI models. Furthermore, there are few standardized applications of 3D city models with VGI (Goetz and Zipf, 2011). Some official spatial data include 3D VGI data to plan and manage urban environments (Sheppard and Cizek, 2009). This brings up potential risks, such as error reproduction and even legal concerns. Many methods have been proposed to examine these VGI data qualities via developing Web-based community forums which allow creators and users to discuss and update. They are similar with most shopping websites and other commercial websites, such as Amazon, App store, and Priceline. More and more people post large amount of reviews every day, every hour, and even every second, which somehow is as standard of online information quality. The quality of such online information can be called “perceived quality” which is an expression of users’ perspectives (Jones, 2011). Jones (2011) propose the five-star method to express the quality of spatial data (Figure 1). A 3D model is created by User 1 via SketchUp (an online application). Afterwards, it is stored into the 3D Warehouse which is the access to allow other users use this 3D model. Depending on experiences and purposes of use, they will write commends to assess this 3D model from User 1 and give a star-level standard. Finally, an average assessment is provided and posted so that other new users can view this assessment before use. Figure 1 illustrates the assessment. However, perceived quality focuses only on external applications that are related with users’

experience and their purpose. The quality of 3D VGI models is associated to not only external applications but also internal data quality. This thesis introduces a method of assessing the quality of 3D VGI models extracted by a Web 2.0 tool – Google Building Maker.

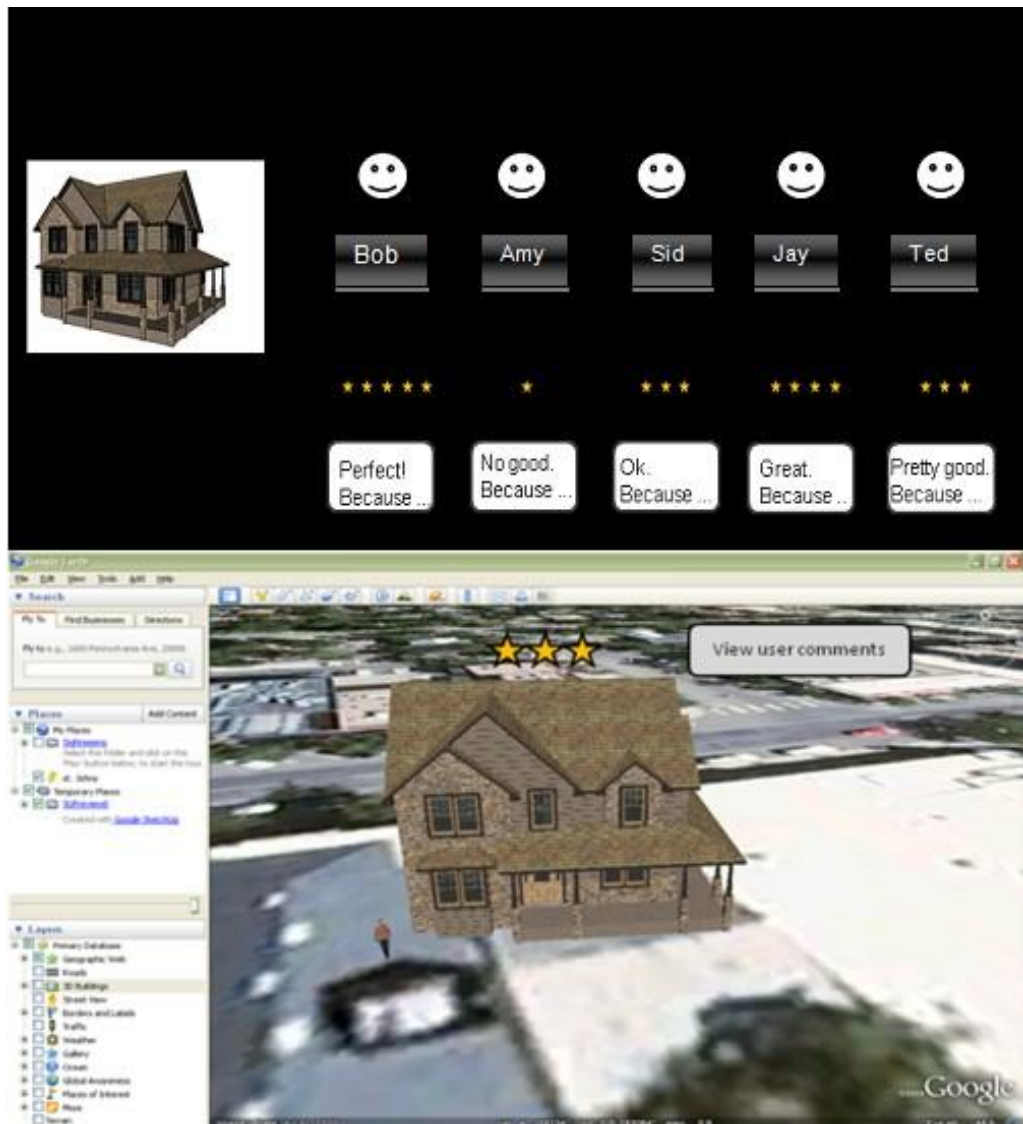


Figure 1. Perceived quality evaluation and average rating visualization. (Jones, 2011)

CHAPTER 3

STUDY AREA, DATA, SOFTWARE, AND BASIC KNOWLEDGE

Study Area

A group of parcels with 19 buildings near Mowry Avenue in the City of Fremont, California was selected as the study area (Figure 2 (a), (b), & (c)). Figure2 (a) displays overall nDSM of Fremont city; Figure2 (b) is aerial image which is zoomed in on the study area; and Figure2 (c) show the nDSM that is zoomed in on the study area. This study area was chosen because the buildings in the group cover all common types of roofs, such as flat roof, shed roof, gable roof, mansard roof, and hip roof (Figure 3).

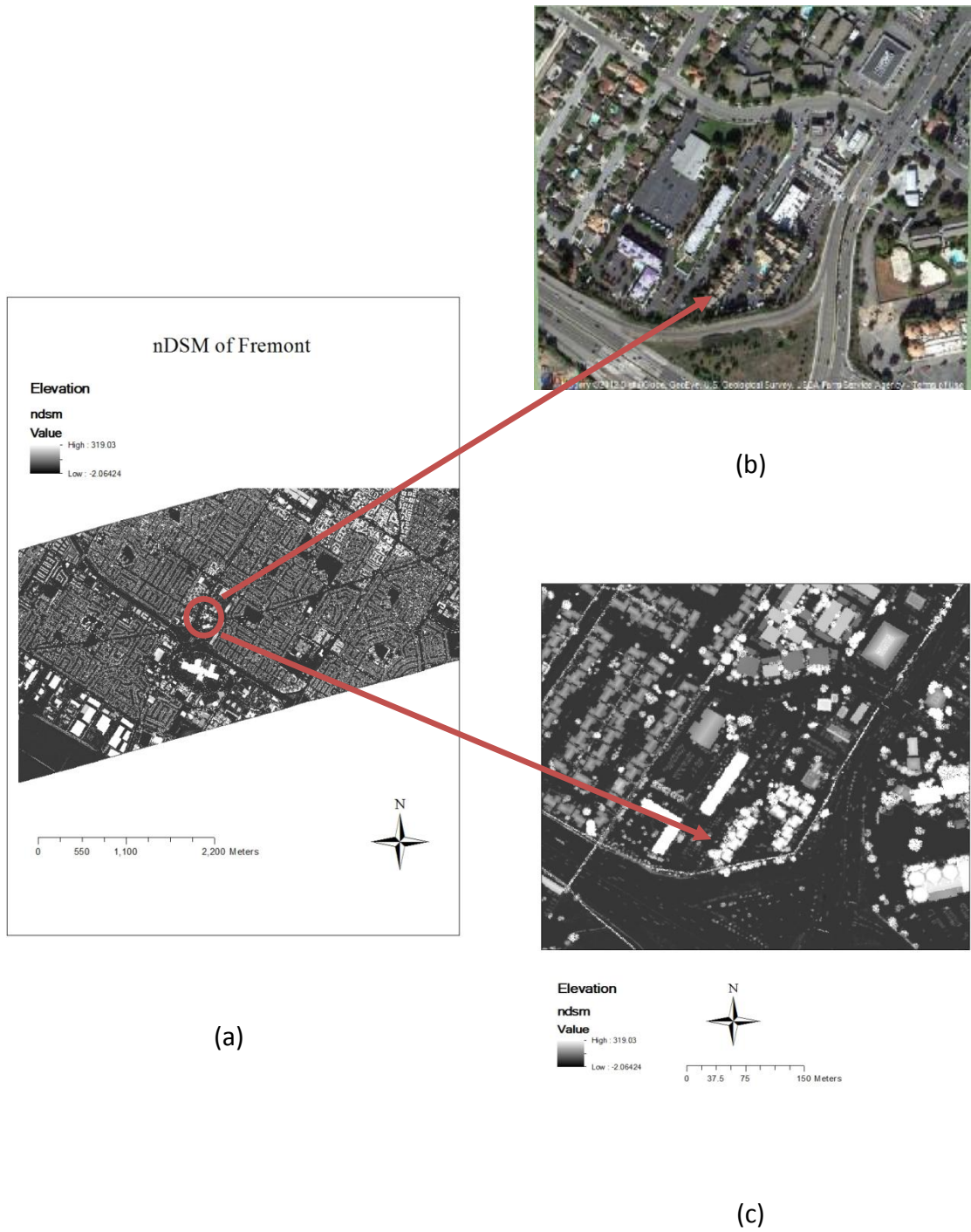
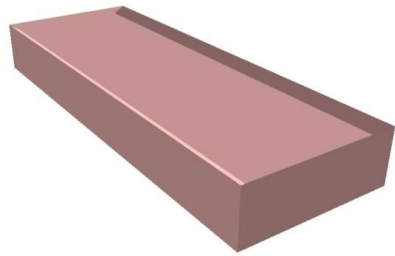
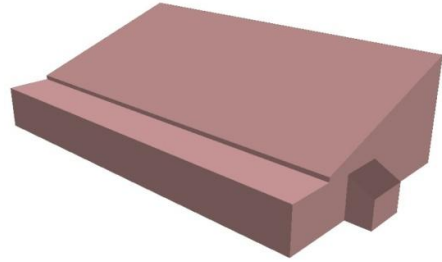


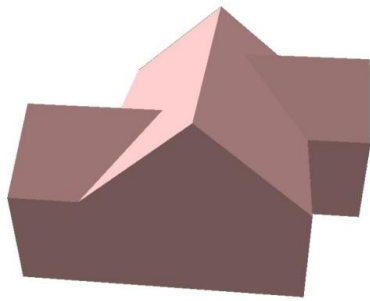
Figure 2. LiDAR nDSM (a and c) and Google image (b) of the study area.



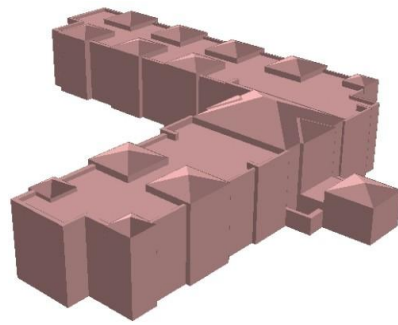
(a) Flat roof



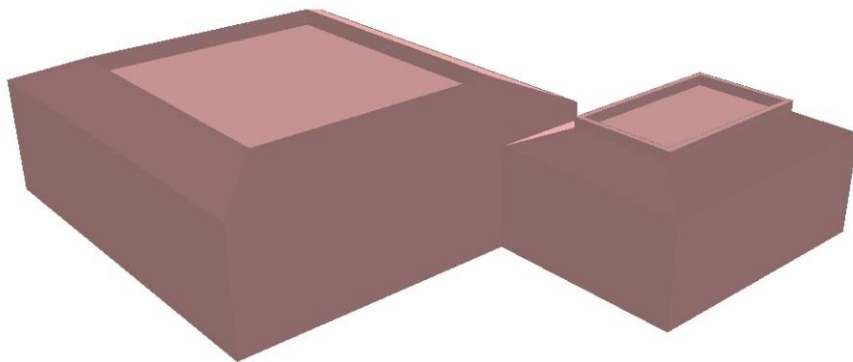
(b) Shed roof



(c) Gable roof



(d) Hip roof



(e) Desk roof

Figure 3. Five roof types: (a) flat; (b) shed; (c) gable; (d) hip; (e) desk.

Data

The data acquired for this project are:

- (1) High-resolution imagery: The high-resolution images are from Google Maps. The high-resolution images of cities include aerial photographs that are taken by aircraft flying at 800–1500 feet; while most of other images are collected from satellites (Google earth, 2012). The high-resolution images from Google Maps are used for manual extraction of 3D VGI building models.
- (2) LiDAR data: The LiDAR data are collected by the NSF GeoEarthScope project, and downloaded from the OpenTopography Cyberinfrastructure at the San Diego Super Computer Center.

Software Tools

In this study, three software packages are used for data collection, data pre-processing, and data analysis.

- (1) Google Building Maker: It is a 3D Web-based application for creating 3D building models (Google, 2009). Building models are extracted as simple geometric shapes from aerial photos supplied by Google. Once submitted to the Google Building Warehouse, these building models will be evaluated by Google in a few days. If the quality of building models is good enough, Google will confirm them via E-mail and share them for public use.

- (2) SketchUp: It is launched by @Last Software in 1999. Google as a developer releases this software in August 2000. Although there are a few features not available from the free version of SketchUp, it is enough for creating and editing simple 3D building shells. The SketchUp software is updated almost every year. In this study, SketchUp 8 is employed for editing 3D building models created from Google Building Maker. New released features, such as geo-location with Google Maps, Outer Shell, and matching aerial photos, improve the quality of 3D VGI building models collected by Google Building Maker.
- (3) ArcGIS 10: ArcGIS 10 is used to: (a) convert 3D building models into GIS data for further editing; (b) pre-process LiDAR data to create normalized digital surface models (nDSM);and (c) compare 3D building models generated from Google Building Maker and LiDAR data.

Basic Terms Related To Data and Software

- (1) COLLADA format: Its full name is a collaborative design activity which establishes “an open standard digital asset schema for interactive 3D applications” (COLLADA, 2007). It is an XML database schema that allows free exchange of 3D applications without losing any information. Google Earth files and 3D geometric shapes in the 3D Google Warehouse are in COLLADA format which can be changed to other formats easily (Google SketchUp Blog, 2009).

(2) Multipatch: A multipatch is a shapefile consisting of a series of surface polygons.

It allows simplifying complex buildings and appending textures on surfaces. The newer ArcGIS edition, ArcGIS 10, provides new features allowing creating and managing multipatch data. A COLLADA file can be directly changed into multipatch format and viewed in 3D (Table 2: Multipatch 3D models). A series of editing features, including Move, Rotate, and Scale, help revise the new multipatch layer on the landscape. Besides, a new function of the 3D Analysis in ArcGIS 10 is automatically displaying textures on surfaces.

(3) nDSM: nDSM is a normalized digital surface model, which is the difference between a digital elevation model (DEM contains the terrain's elevations over a bare area) and a digital surface model (DSM presents the elevations of both terrains and objects' surfaces on terrains). In fact, an nDSM has elevations of objects on the bare earth surface. nDSM is a raster dataset or a triangular irregular network (TIN). The triangulation process refers that all raw LiDAR points are connected in a network consisting of triangular faces. An example of TIN is shown in Figure 4.

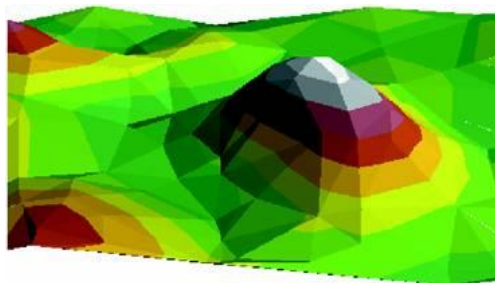


Figure 4. An example of a TIN.

CHAPTER 4

METHODOLOGY

Collecting 3D VGI models

3D data in GIS contain x, y and z axes (Hudson-Smith and Evans, 2003). Unlike natural landscape features, buildings created by humans are relatively regular. Moreover, man-made structures are better represented in 3D of vector models (Alexander et al, 2009). 3D geometric shapes are normally constructed by existing GIS, AutoCAD, and photogrammetry methods. In this study, 3D geometric shapes of buildings are extracted from Google Building Maker. Figure 5 shows the processes of extracting 3D buildings using Google Building Maker and SketchUp.

The major steps are described below:

- (1) Select the location of interest in Google Building Maker via the geo-location function of SketchUp (Figure 6).
- (2) Go to Google Building Maker web-page and add 3D geometric shapes from different angles (Figure 7).
- (3) Export the extracted building models into the SketchUp interface.

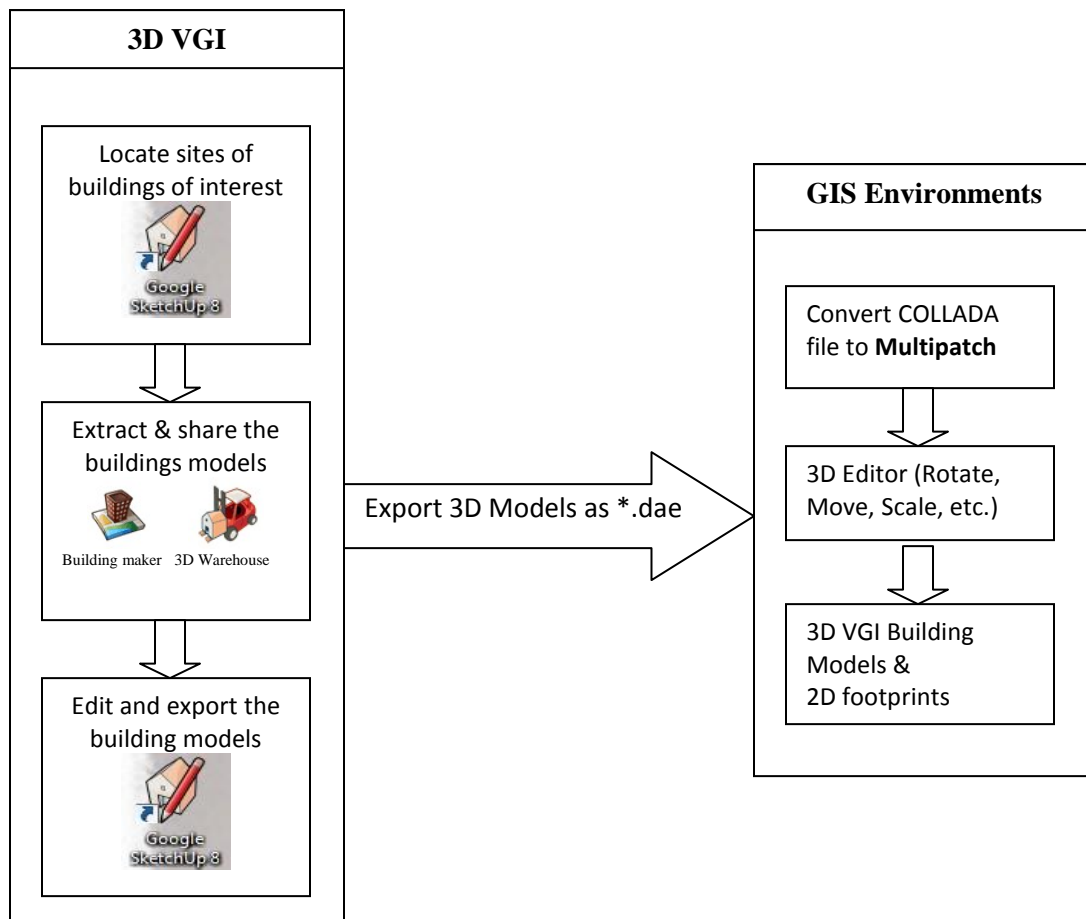


Figure 5. Flowchart for generating 3D VGI models and exporting to ArcGIS environment.

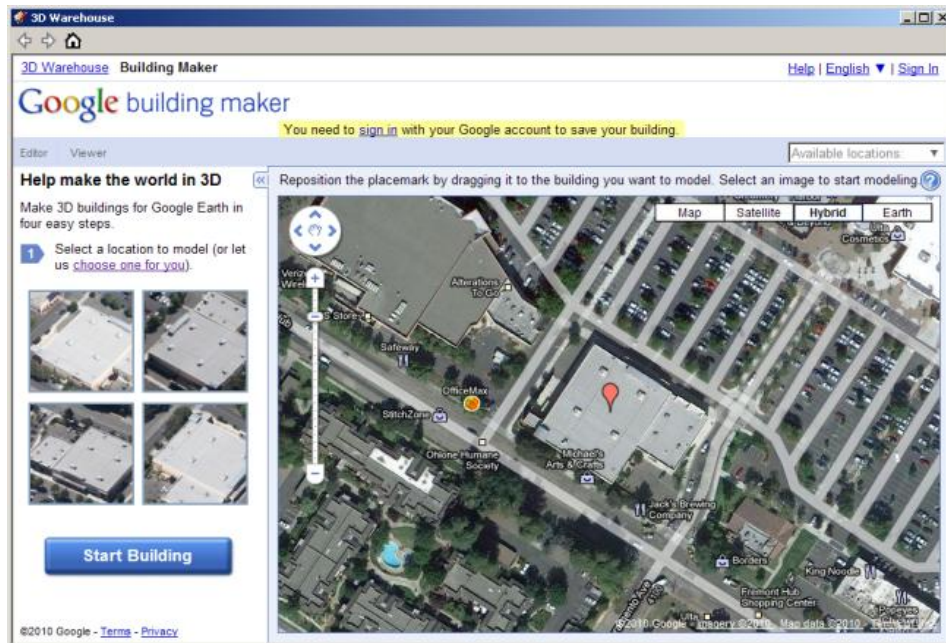


Figure 6. Locating buildings in Google Building Maker.

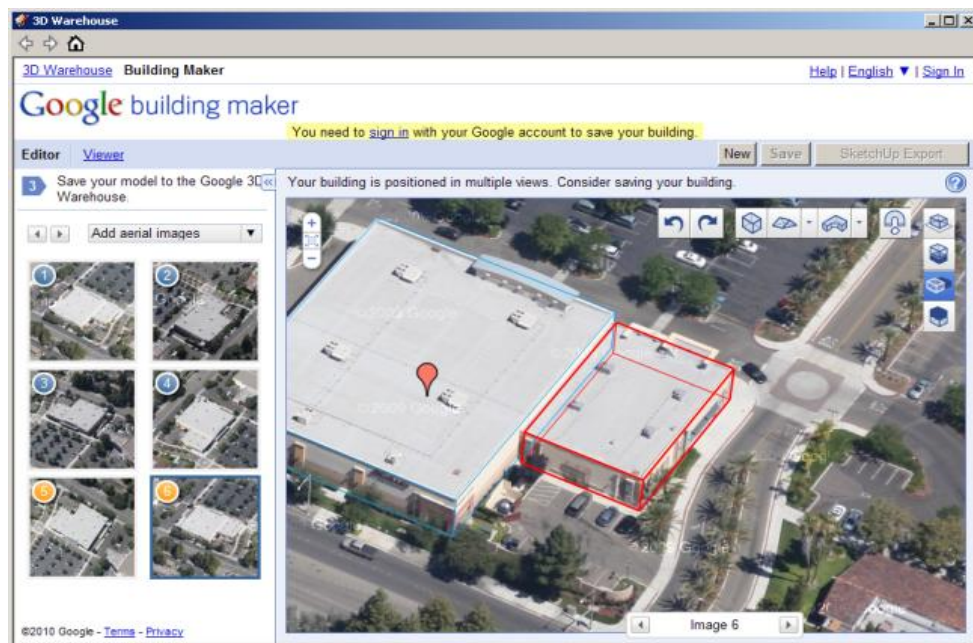


Figure 7. Adding 3D geometric shapes in Google Building Maker.

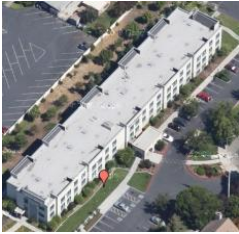

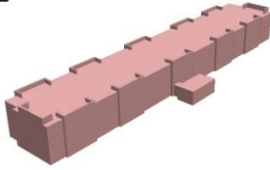


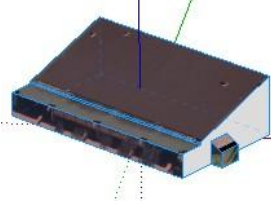
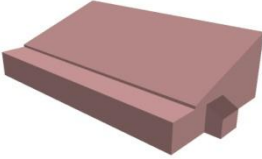
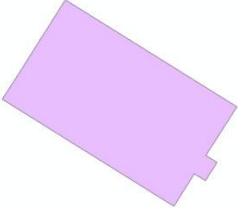
(4) The 3D models are edited in Google SketchUp, and the Outer Shell tool is used to solid geometries so that the gaps and single segments on geometries could be removed and cleaned up. After deriving the original building models, a series of building models are created by increasing or decreasing the height and width of each original building by 5%, 10%, 15%, 20%, 25%, and 50%. This is to simulate errors induced by ordinary Internet users when creating the 3D building models through Google Building Maker.

(5) Afterwards, these 3D VGI building models are exported as COLLADA files;

(6) Finally, the COLLADA files are converted to multipatch shapefiles in ArcGIS 10.

For example, Table 2 illustrates the conversion from Sketchup 3D geometric shapes to GIS multipatch shapefiles.

Table 2. Conversion from COLLADA File to Multipatch File.

High resolution	3D model of the	Multipatch 3D	Ortho-view of
			
			

Extracting LiDAR nDSM

LiDAR data are represented by a set of points, and the dataset is sized by the range of the scanning area (Alexander et al, 2009). There are many automatic methods for extracting building footprints from LiDAR DEM. In this study, the multipatch footprint of each building was assumed to be available. These multipatch footprints not only provide the areas of buildings, but also are used as masks for extracting the nDSM of each building. Figure 8(a) and (b) show footprints of two buildings generated from an nDSM.

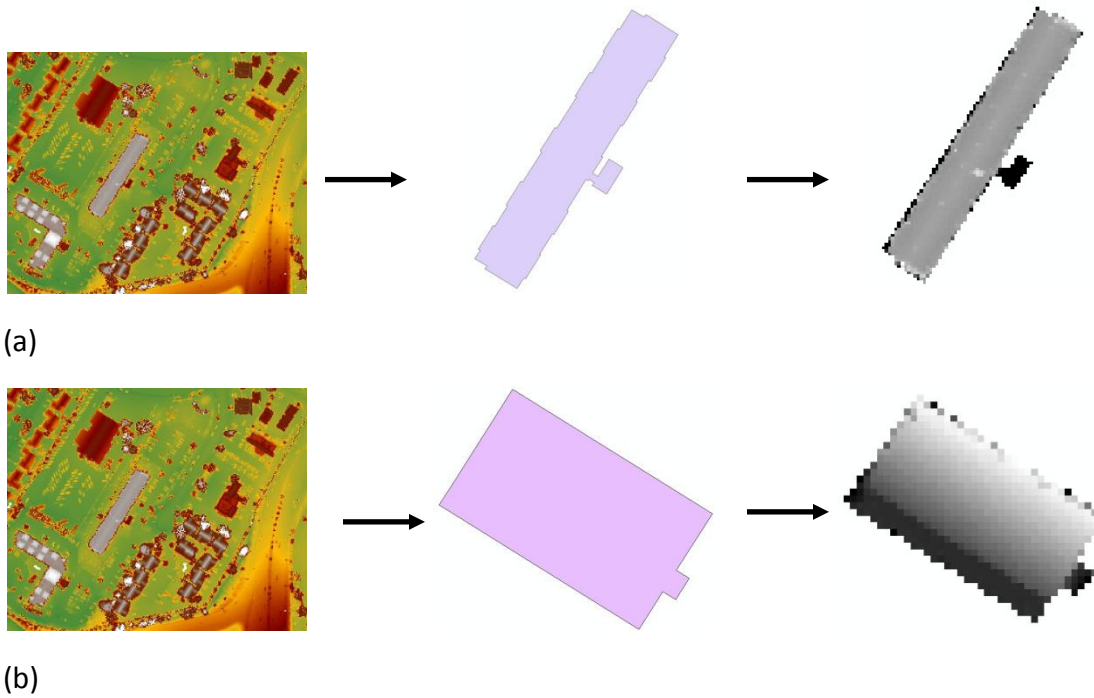


Figure 8. Extraction of building footprints from LiDAR data.

Comparisons of 3D shape signatures

According to Osada et al. (2002), 3D shape signatures are used for measuring the similarity or dissimilarity between 3D shapes. The fundamental principle of 3D shape signatures is converting 3D geometric shapes to parameterized functions so that the 3D objects can be easily analyzed (Osada et al., 2002; Dong and Guo, 2011). The 3D geometric shapes are represented by probability distributions derived from geometric functions. Osada et al. (2002) used five functions in their work, namely the angle formed by three random points, the distance between fixed points and random points on 3D model surfaces, the distance between two random points, the square root of the area of the triangle between three points, and the cube root of the volume of the tetrahedron

between four points. Dong (2009, 2010) used one function, the distance between two random points selected from LiDAR data, to create 3D shape signatures of individual tree crowns based on 10,000 pairs of random points so that the 3D shape signatures of the individual tree crown are stable.

In this study, 3D shape signatures are calculated from 3D points on the surface of building models derived from Google Building Maker and LiDAR data. On the walls of building models where LiDAR data point are not available, random points are generated in each triangle in the Triangulated Irregular Network (TIN) using barycentric coordinates (Bradley, 2007). If $p_1(x_1, y_1, z_1)$, $p_2(x_2, y_2, z_2)$, and $p_3(x_3, y_3, z_3)$ are three vertices of a triangle (Figure 9), a random point $p(x, y, z)$ can be calculated using the following equation:

$$p = t_1p_1 + t_2p_2 + t_3p_3 \quad (1)$$

where t_1 , t_2 , and t_3 are barycentric coordinates (Bradley, 2007) and $t_1 + t_2 + t_3 = 1$.

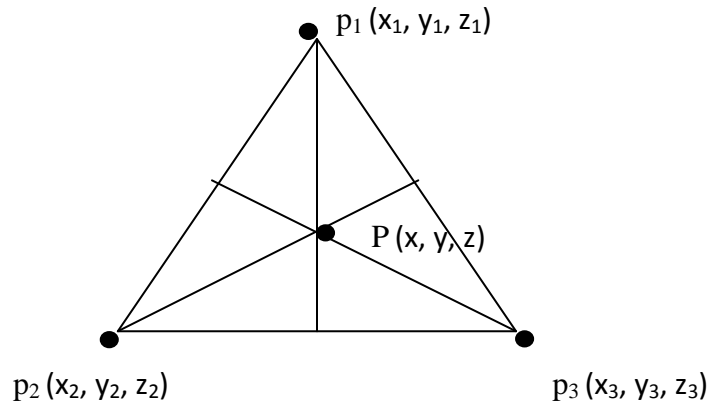


Figure 9. Barycentric coordinates inside a triangle.

In the work of Dong (2009, 2010), there are 10,000 pairs of random points for creating 3D shape signatures of tree crowns. Since buildings are more complex than nature features, 100,000 pairs of random points were used to generate 3D shape signatures for each building in this study. An interesting issue is to select shape functions whose distributions represent good signatures for the 3D models (Osada et al., 2010). Six shape functions were used: angle, area, aspect, distance, slope, and volume. These shape functions can be sampled to form shape distributions. Specifically, these six functions are explained below, and mathematical expressions of these functions can be found in Liu et al. (2012). The process is shown in Figure 10.

- (1) Angle: the angle between three random points on the surface of a 3D model.
- (2) Area: the area of a triangle consisting of three random points on the surface of a 3D model.
- (3) Aspect: the downslope direction of the triangle between three random points on the surface of a 3D model.
- (4) Distance: the distance between two random points on the surface of a 3D model.
- (5) Slope: the angle between a 3D triangle formed by three random points on the surface of a 3D model and the horizontal plane.
- (6) Volume: the volume of a tetrahedron formed by four random points on the surface of a 3D model.

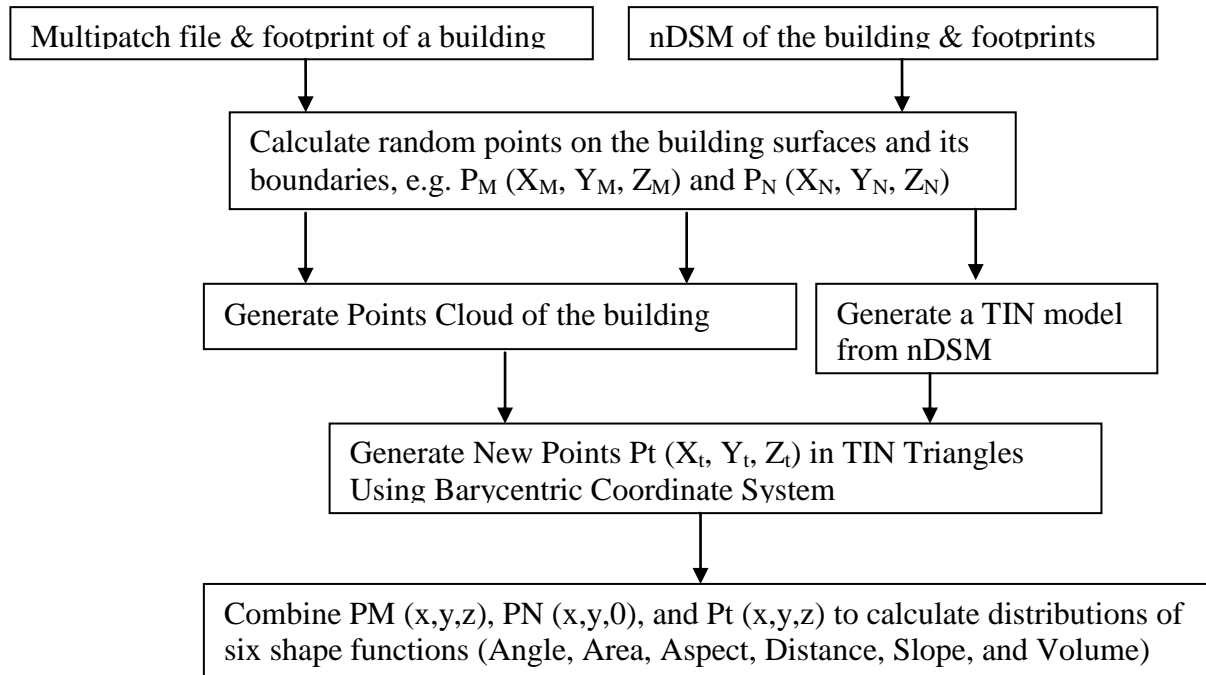


Figure 10 . Flowchart of 3D shape signature analysis.

The method described above was implemented using C# and ArcObjects for ArcGIS 10 for comparison between LiDAR-derived 3D building models and user-generated 3D building models created using Google Building Maker.

CHAPTER 5

RESULTS ANALYSIS

3D Shape Distribution Results

Figure 11 shows that the 3D building models in the study area displayed in Google Earth. The 3D Buildings models in the study area are represented as TIN generated from nDSM (Figure 12). Meanwhile they are represented through Multipatch files converted from COLLADA files (Figure 13). In order to evaluate the similarity of 3D LiDAR models and 3D VGI models, a series of 3D shape signatures are calculated from random points on surfaces of different 3D Models (Figure 18).

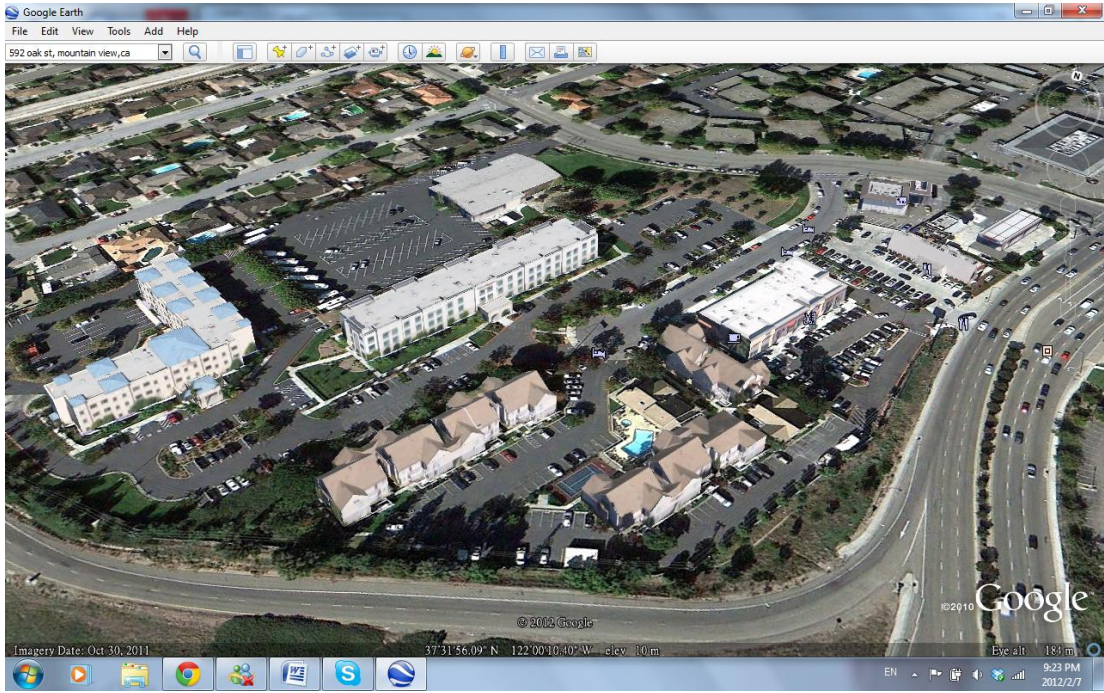


Figure 11. 3D building models via Google Building Maker and displayed on Google Earth.

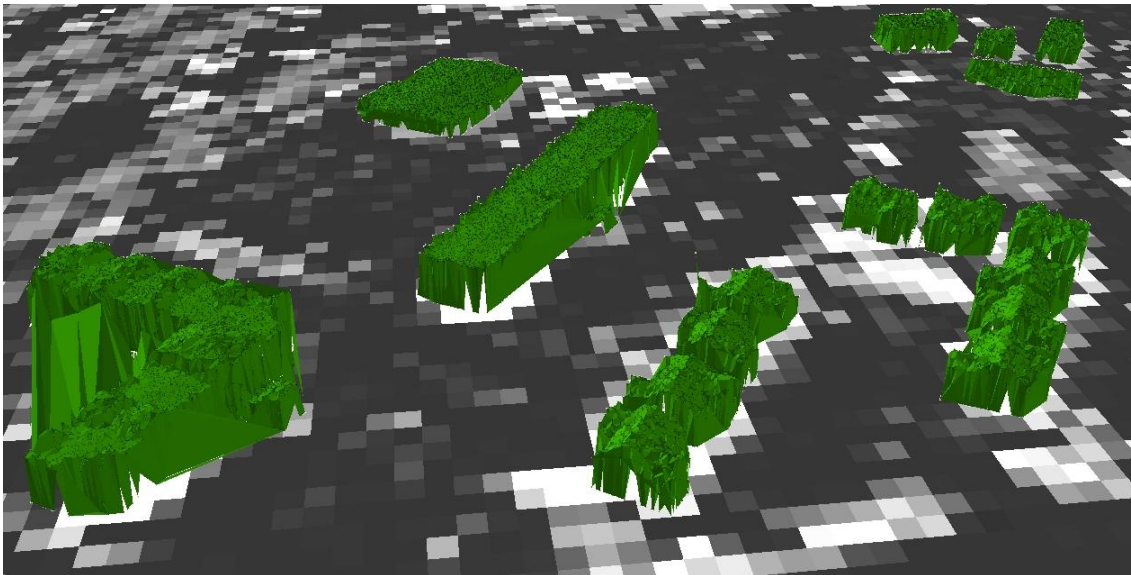


Figure 12. TIN models of LiDAR-derived buildings.

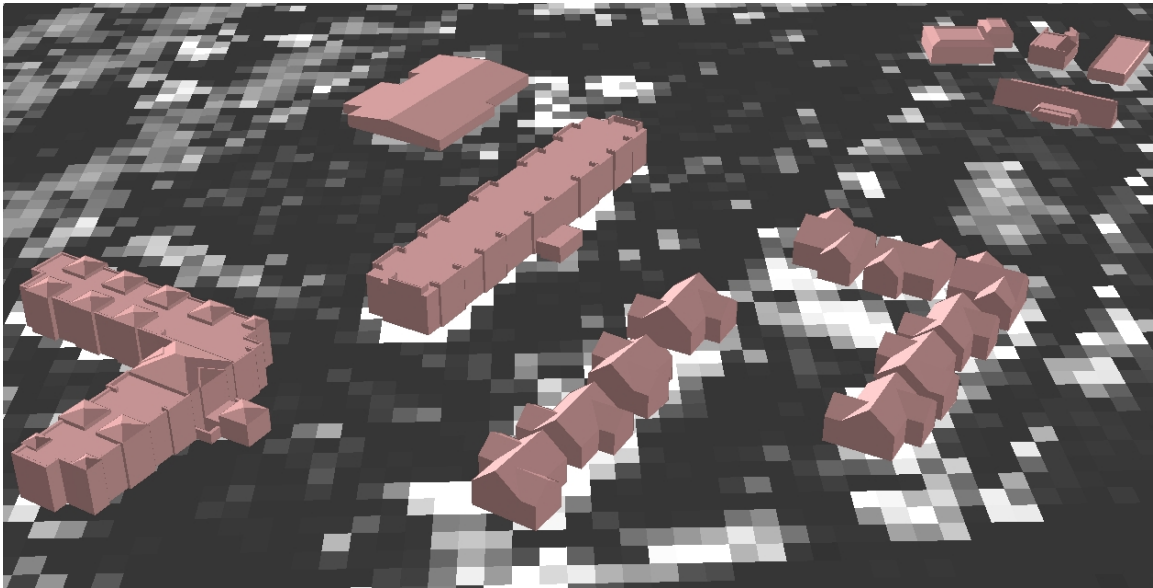


Figure 13. 3D Multipatch models viewed in ArcScene.

Similarity analysis

In Figure 18, each histogram includes two distribution curves: an nDSM distribution curve and a user-generated 3D model's curve. As can be seen in the Figure 20, most 3D shape signatures in the columns for angle, area, distance and volume do not show significant difference between LiDAR-derived 3D building models and user-generated 3D building models. Furthermore, in Table 3, most correlation coefficients (r) for angle, volume, distance, and area functions are greater than 0.98. If only the four shape functions are considered as measures, the shape distributions of most 3D building models are highly correlated. However, from the 3D shape signatures generated based on the other two functions (aspect and slope), many of the user-generated 3D building models have distinctive shape distributions from their LiDAR-Derived 3D building models. Their r values are less than 0.98 in Table 3.

To investigate why there are differences between user-generated 3D models and their LiDAR nDSM, it is possible to analyze their 3D geometric models. For example, comparing B3 TIN (Figure 14 (b)) with B3 multipatch (Figure 14 (a)), the upper right corner protrudes from the B3's roof; whereas, the B3 multipatch has a flat roof without that protruding corner. Other examples as same as B3, B4 (Figure 15) and B6 (Figure 16), have the same problem when comparing their multipatches to their TIN models. The noises impact the shape distributions for LiDAR-Derived 3D building models; thereby weakening accuracy of the measure.



Figure 14. 3D B3 Models: (a) User-generated 3D model; (b) TIN model from LiDAR.

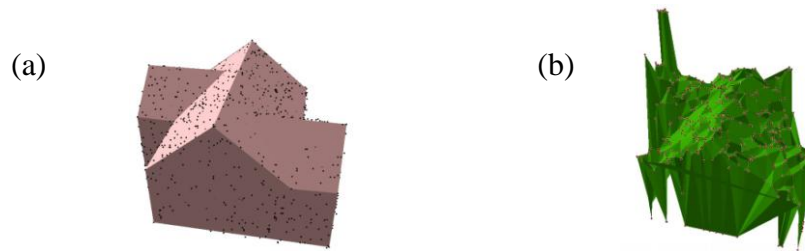


Figure 15. 3D B4 Models: (a) User-generated 3D model; (b) TIN model from LiDAR.



Figure 16. 3D B6 Models: (a) User-generated 3D model; (b) TIN model from LiDAR.

In addition, complex buildings, such as B1 (Figure 17.a), B2 (Figure 17.b), B16 (Figure 17.c), and B18 (Figure 17.d), contain irregular geometric shapes. It is inevitable to get low quality of user-generated 3D building models from Google Building Maker. From Figure 20, it is possible to infer the unmatched shape distributions of multipatch of these buildings with their TIN models from LiDAR. For instance, B1's Slope shape distribution, B2's Aspect shape distribution, B16's Aspect and Slope shape distributions, and B18's Slope shape distribution show obvious difference in their multipatch shape signature curves and the LiDAR-derived shape signature curves.

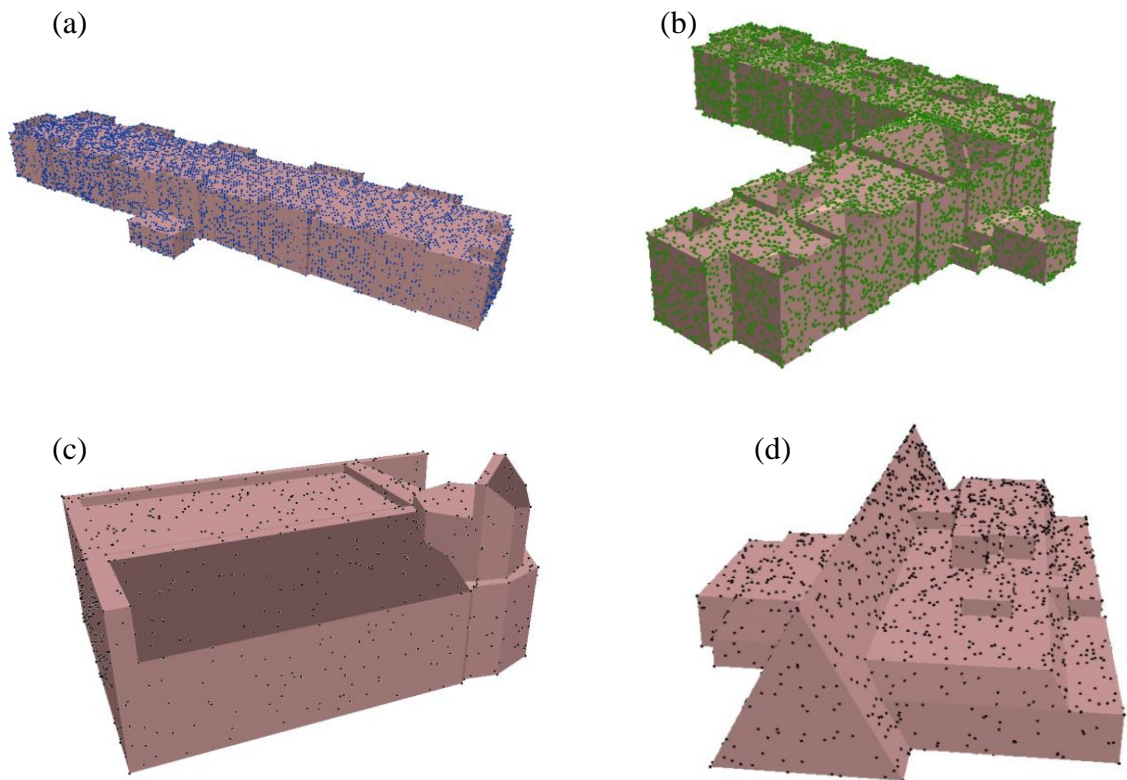
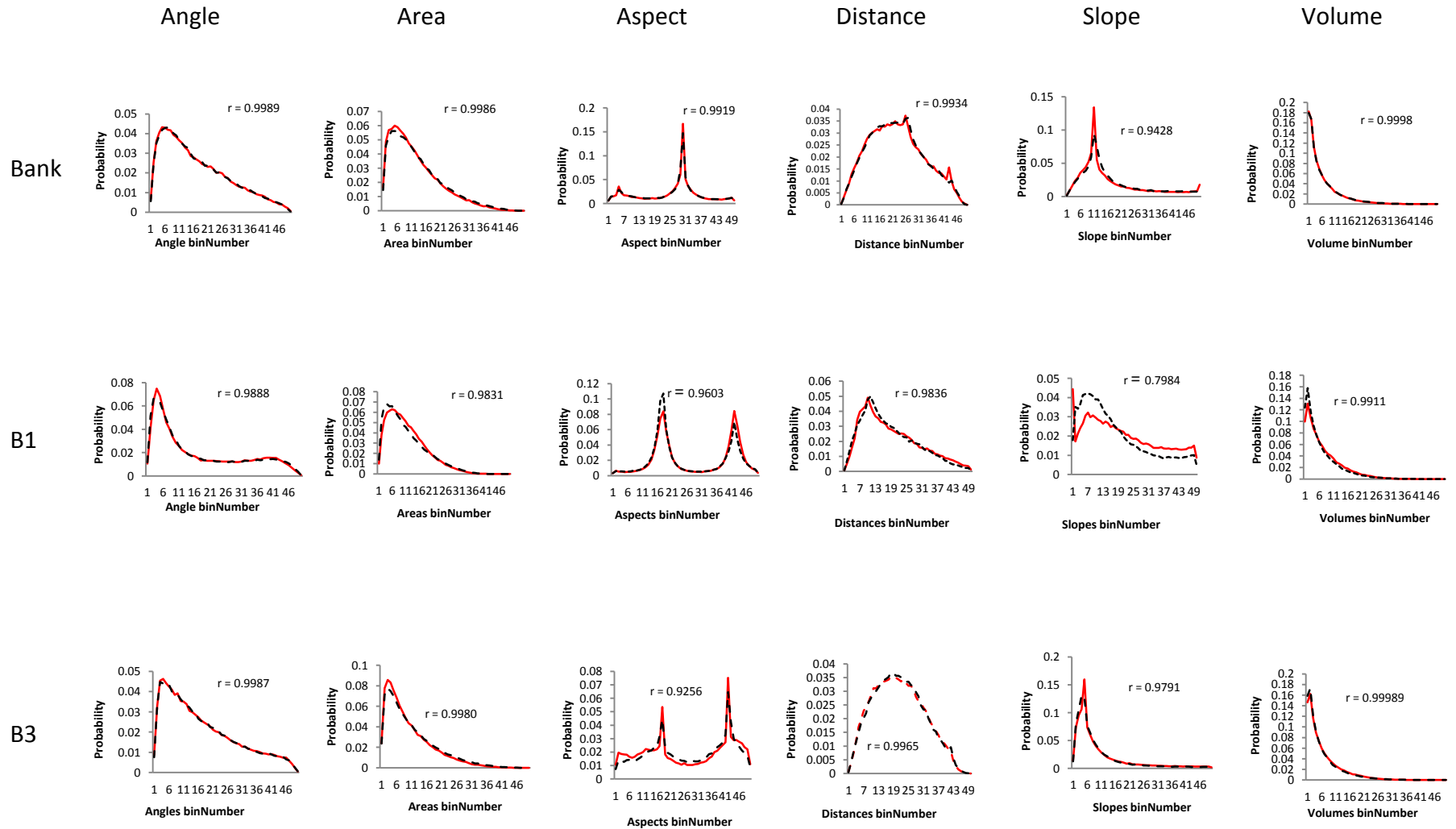
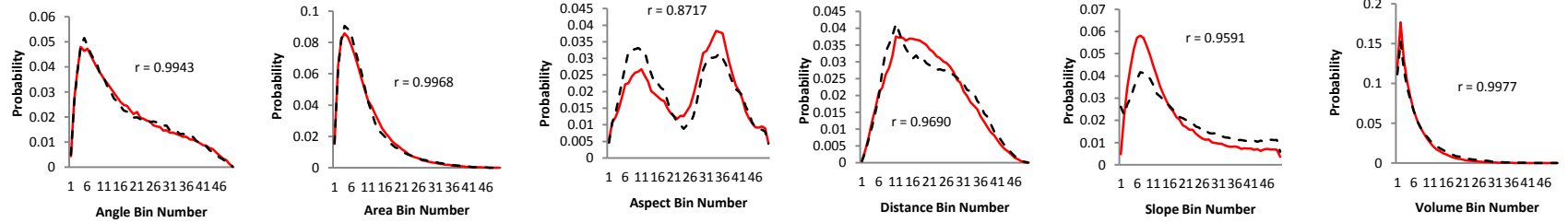


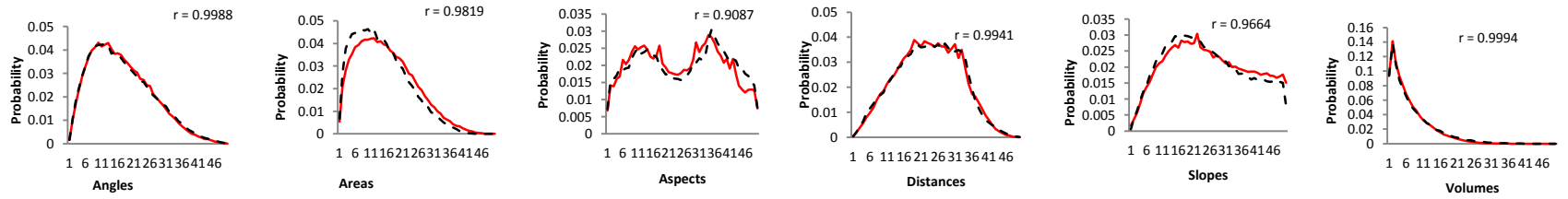
Figure 17. User-generated 3D models: (a) B1; (b) B2; (c) B16; (d) B18.



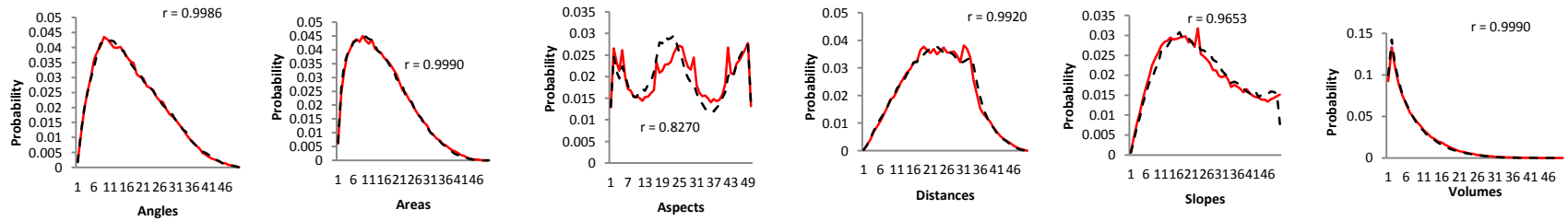
B2



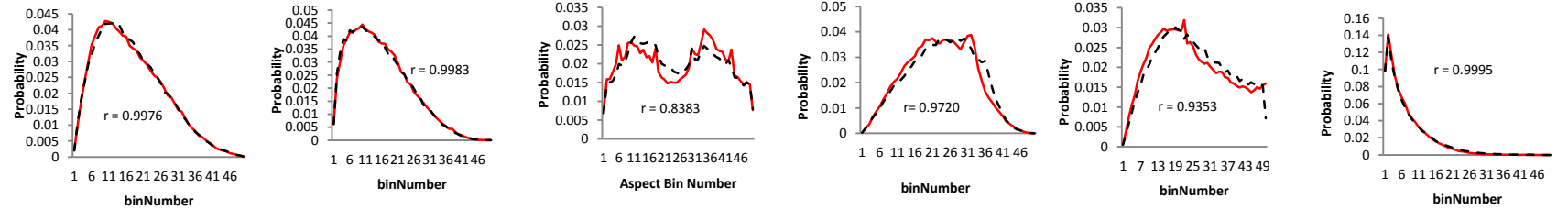
B4



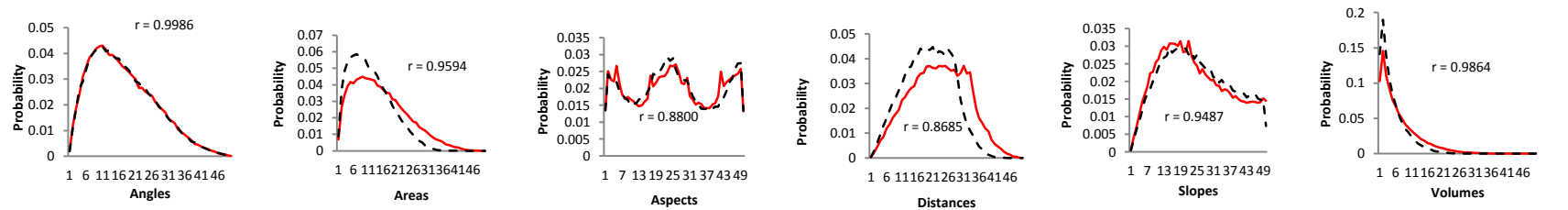
B5



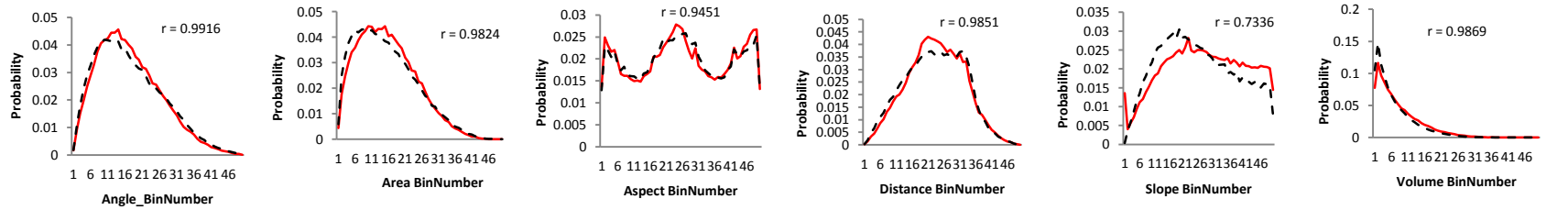
B6



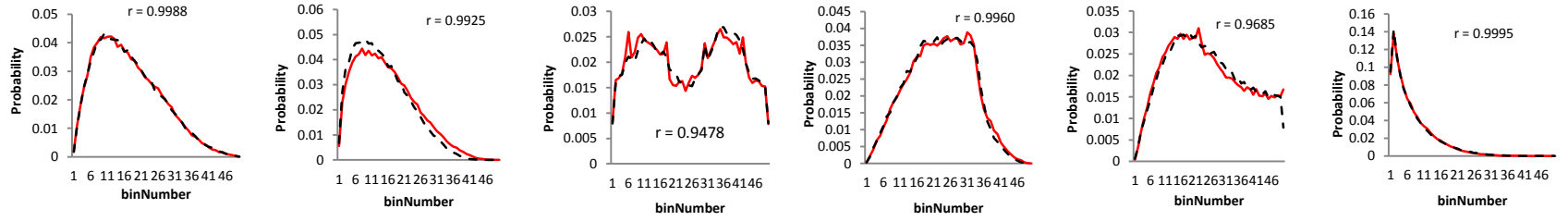
B7



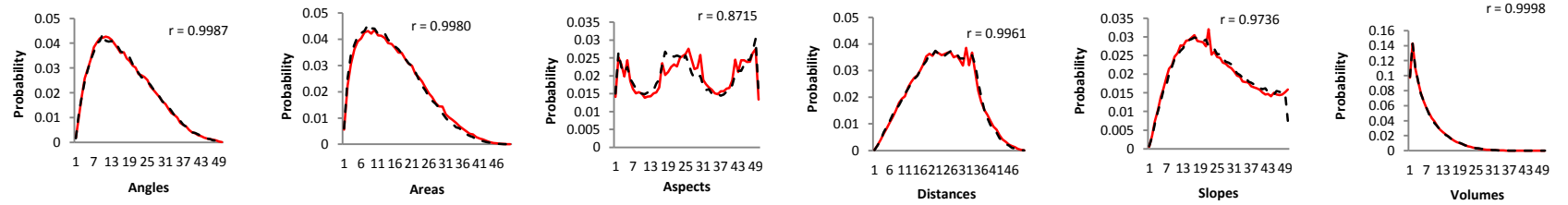
B8



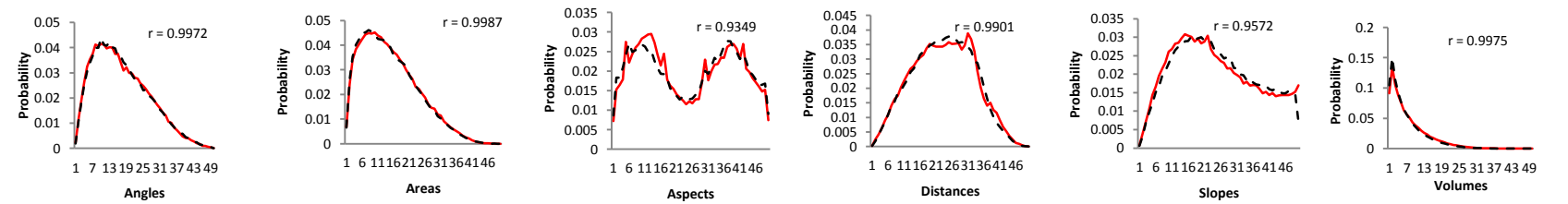
B9



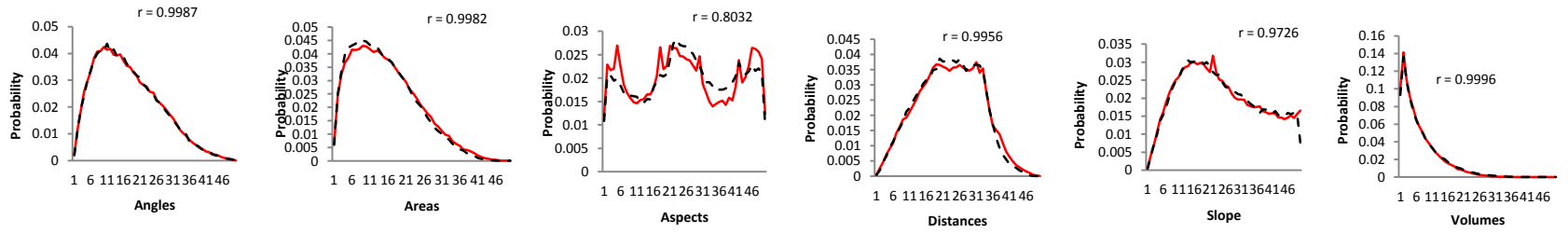
B10



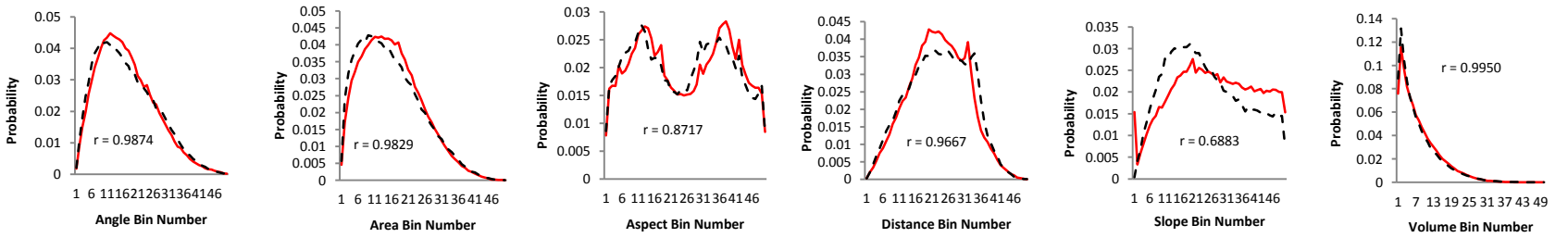
B11



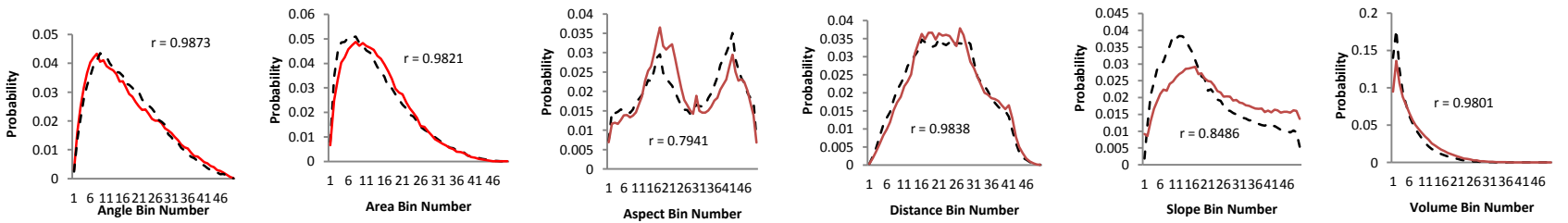
B12



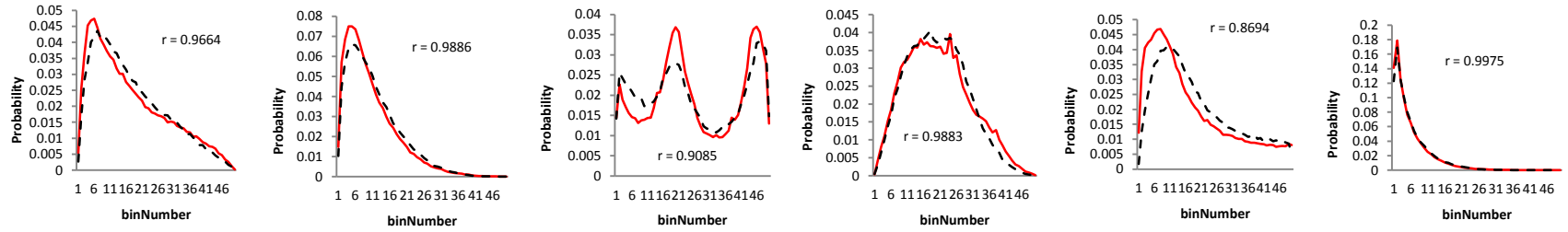
B13



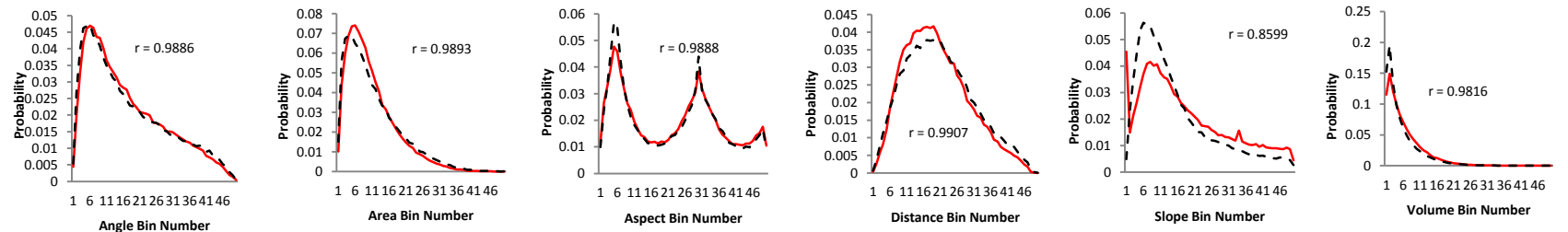
B16



B17



B18



B19

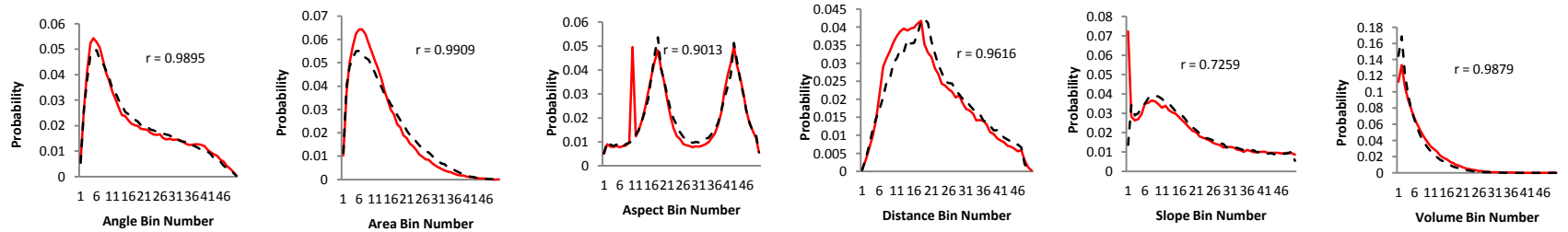


Figure 18. Comparison of 3D shape signatures between LiDAR-Derived 3D models and user-generated 3D models.

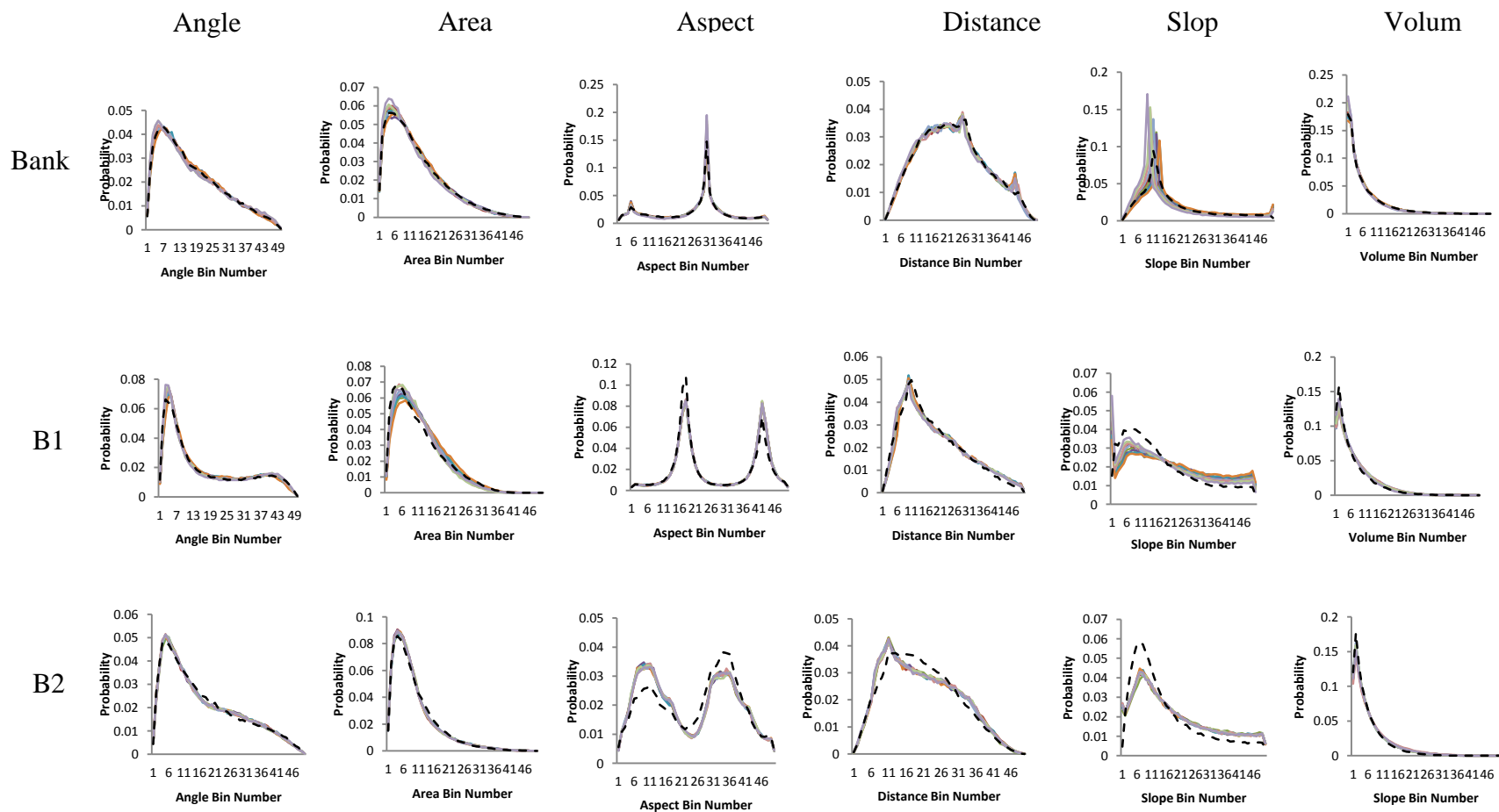
Table3. Correlation Coefficients (r_0) between the 3D Shape Signatures of Figure 18.

	Angle	Area	Aspect	Distance	Slope	Volume
Bank	0.9989	0.9986	0.9919	0.9935	0.9428	0.9998
B1	0.9888	0.9831	0.9603	0.9836	0.7984	0.9911
B2	0.9943	0.9968	0.8717	0.9690	0.9591	0.9977
B3	0.9987	0.9980	0.9256	0.9965	0.9791	0.9999
B4	0.9988	0.9819	0.9087	0.9941	0.9664	0.9994
B5	0.9986	0.9990	0.8270	0.9920	0.9653	0.9990
B6	0.9976	0.9983	0.8383	0.9720	0.9353	0.9995
B7	0.9986	0.9594	0.8800	0.8685	0.9487	0.9864
B8	0.9916	0.9824	0.9451	0.9851	0.7336	0.9869
B9	0.9988	0.9925	0.9478	0.9960	0.9685	0.9995
B10	0.9987	0.9980	0.8715	0.9961	0.9736	0.9998
B11	0.9972	0.9987	0.9349	0.9901	0.9572	0.9975
B12	0.9987	0.9982	0.8032	0.9956	0.9726	0.9996
B13	0.9874	0.9829	0.8717	0.9667	0.6883	0.9950
B16	0.9873	0.9821	0.7941	0.9838	0.8486	0.9801
B17	0.9664	0.9886	0.9085	0.9883	0.8694	0.9976
B18	0.9886	0.9893	0.9888	0.9907	0.8599	0.9816
B19	0.9895	0.9909	0.9013	0.9616	0.7259	0.9879

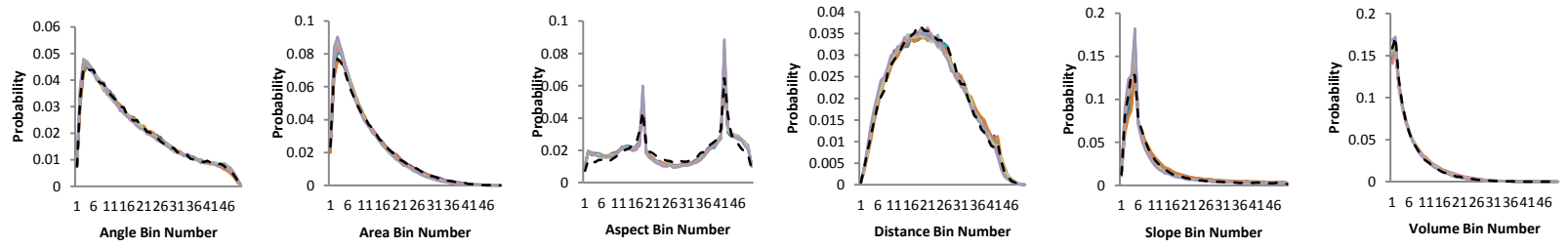
Sensitive Measures

To further test which measures can be used to quantify the differences between LiDAR-derived 3D building models and user-generated 3D building models, the user-generated 3D building models were modified by changing the heights of the roofs from -20% (decrease by 20%) to +20% (increase by 20%), with an interval of 5%. The shape distributions are shown in Figure 19. The correlation coefficients between 3D shape signatures in Figure 19 are also computed. Standard deviations of the correlation coefficients are shown in Figure 20. A higher standard deviation indicates that the

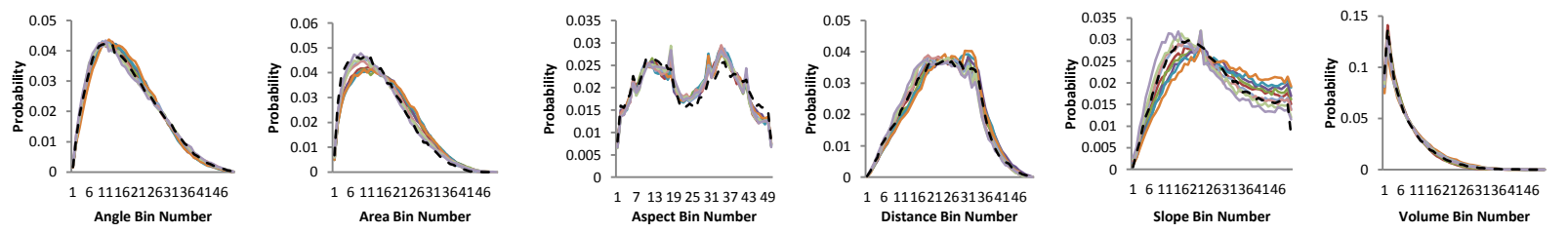
correlation coefficients tend to be more dispersed. As can be seen in Figure 20, over 83% of the cases have high standard deviations of correlation coefficients calculated from the slope function. Although for several cases, the standard deviations of correlation coefficients from the slope function are not the highest, they still appear higher than those from most other shape functions. The results suggest that the slope function is the most sensitive measure of 3D shape signatures among the six functions.



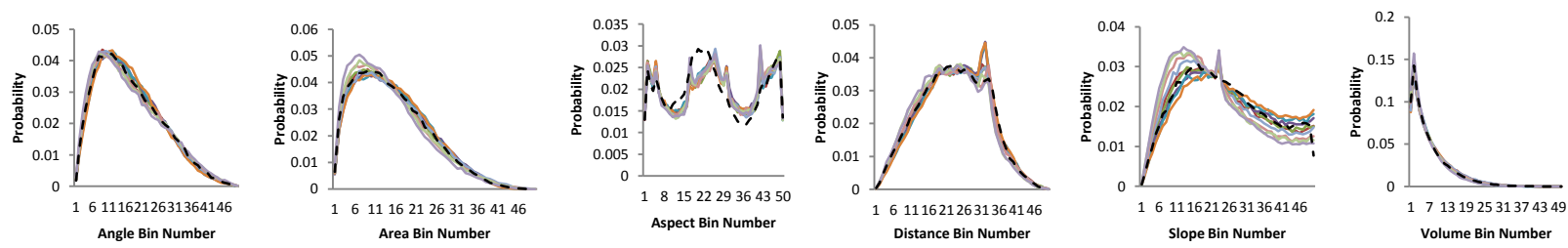
B3



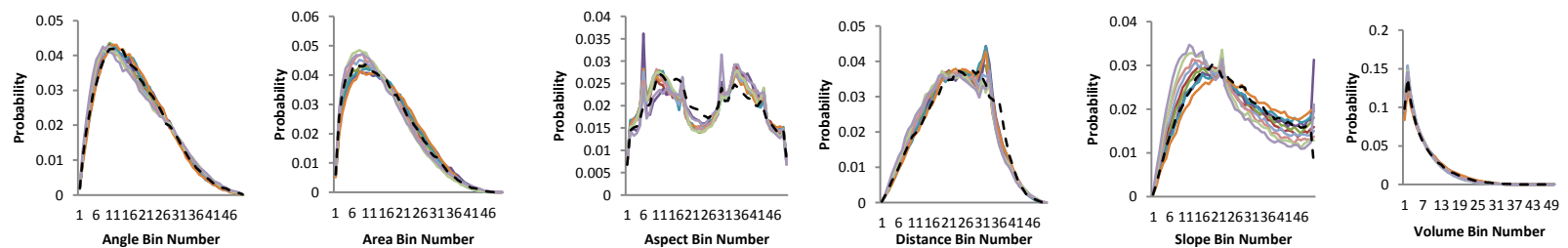
B4



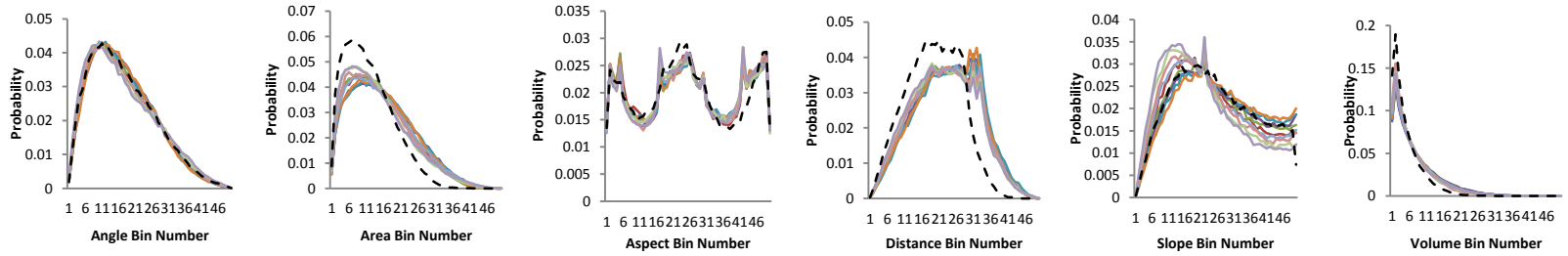
B5



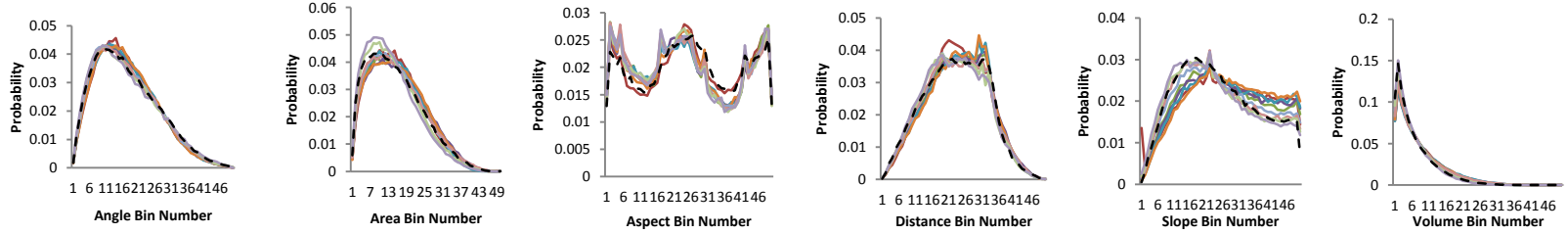
B6



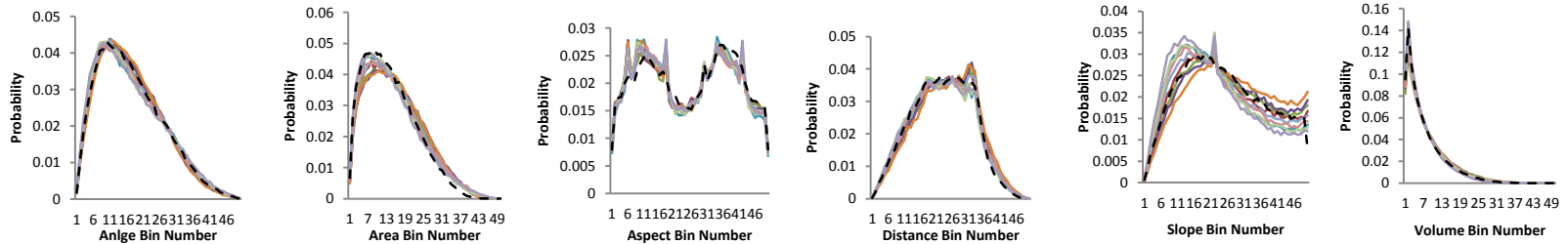
B7



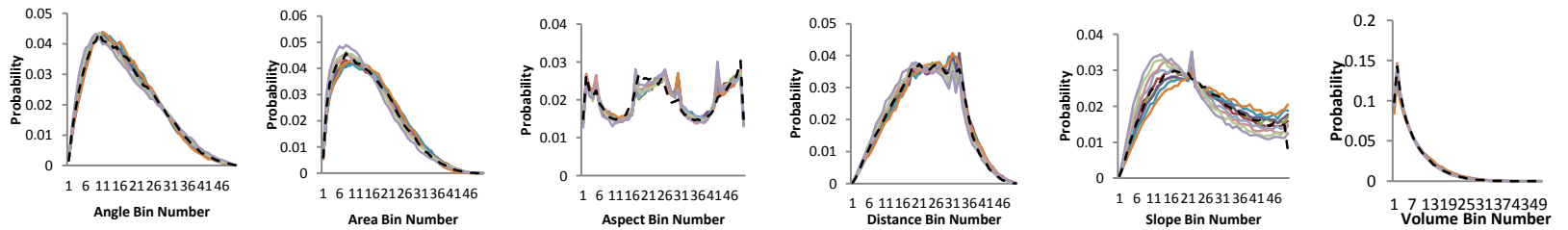
B8



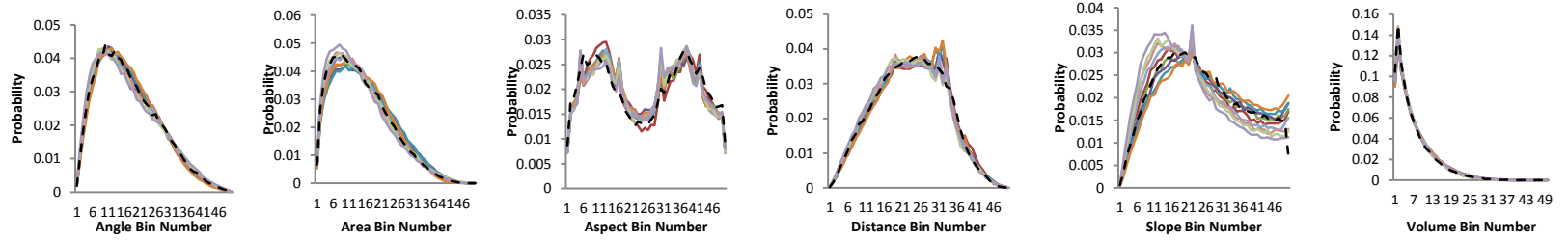
B9



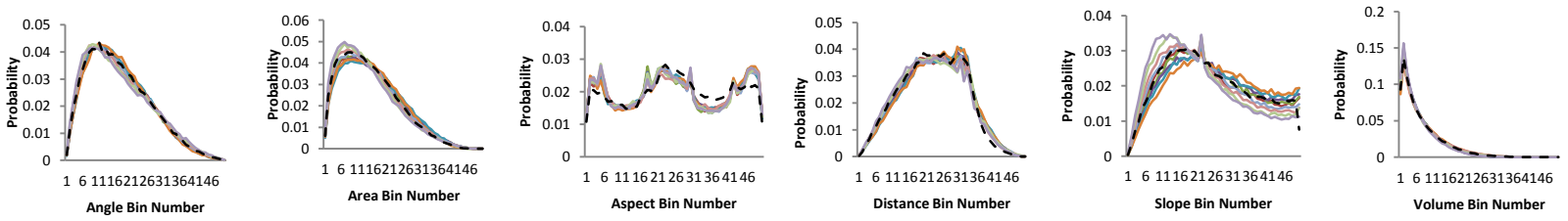
B10



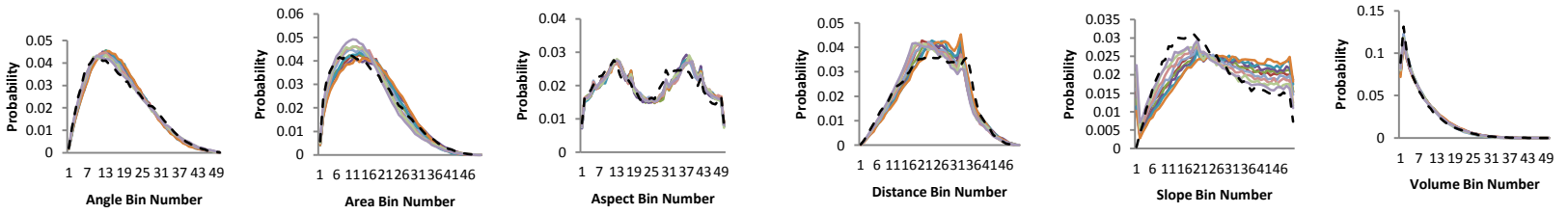
B11



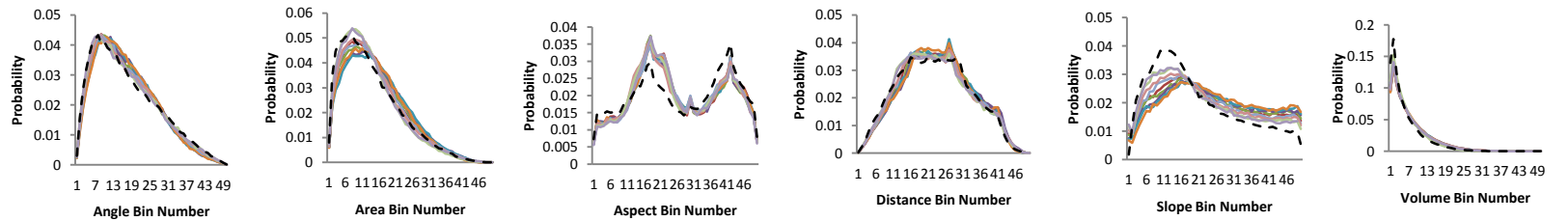
B12



B13



B16



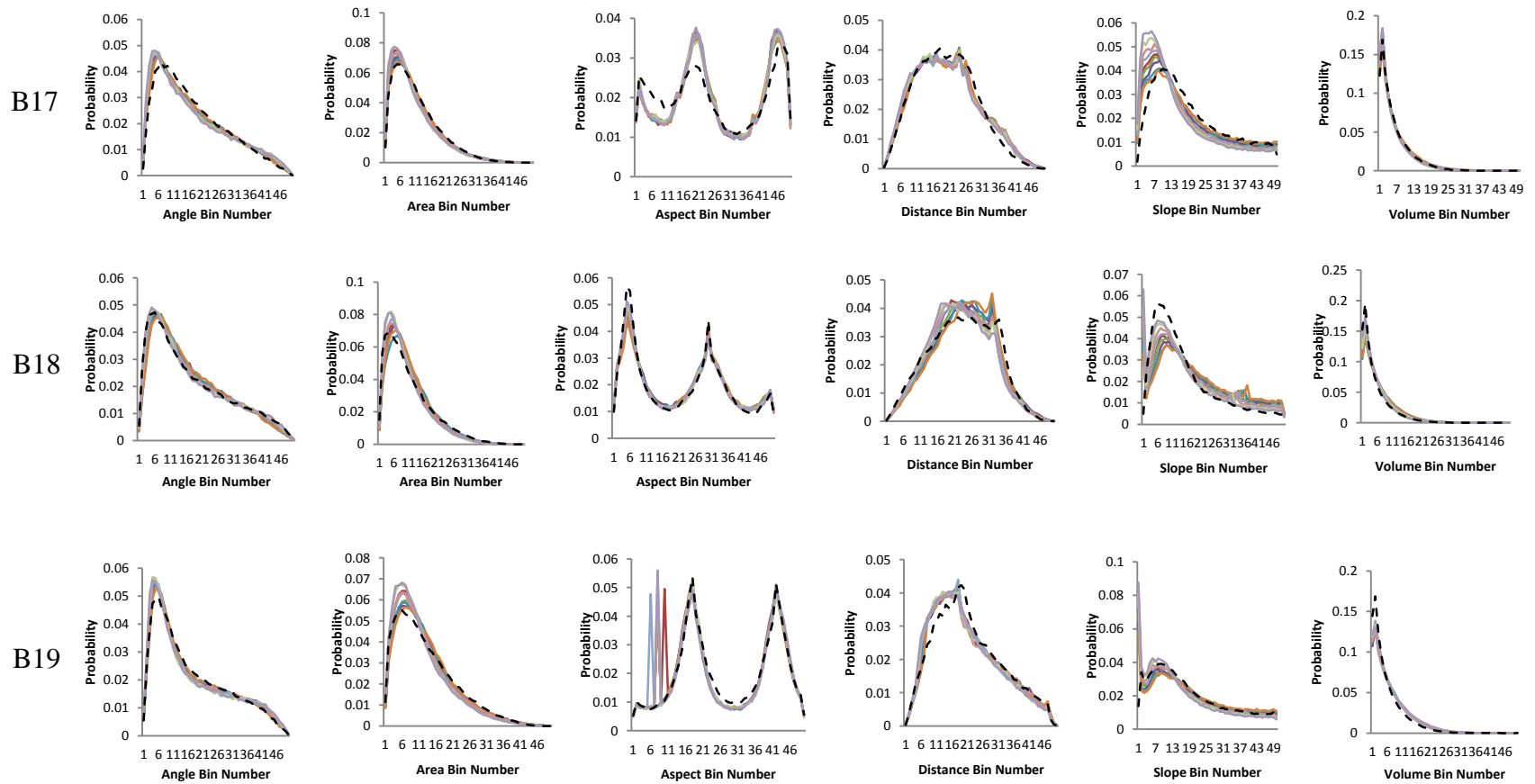


Figure 19. 3D Shape distributions of six functions for 18 building models.

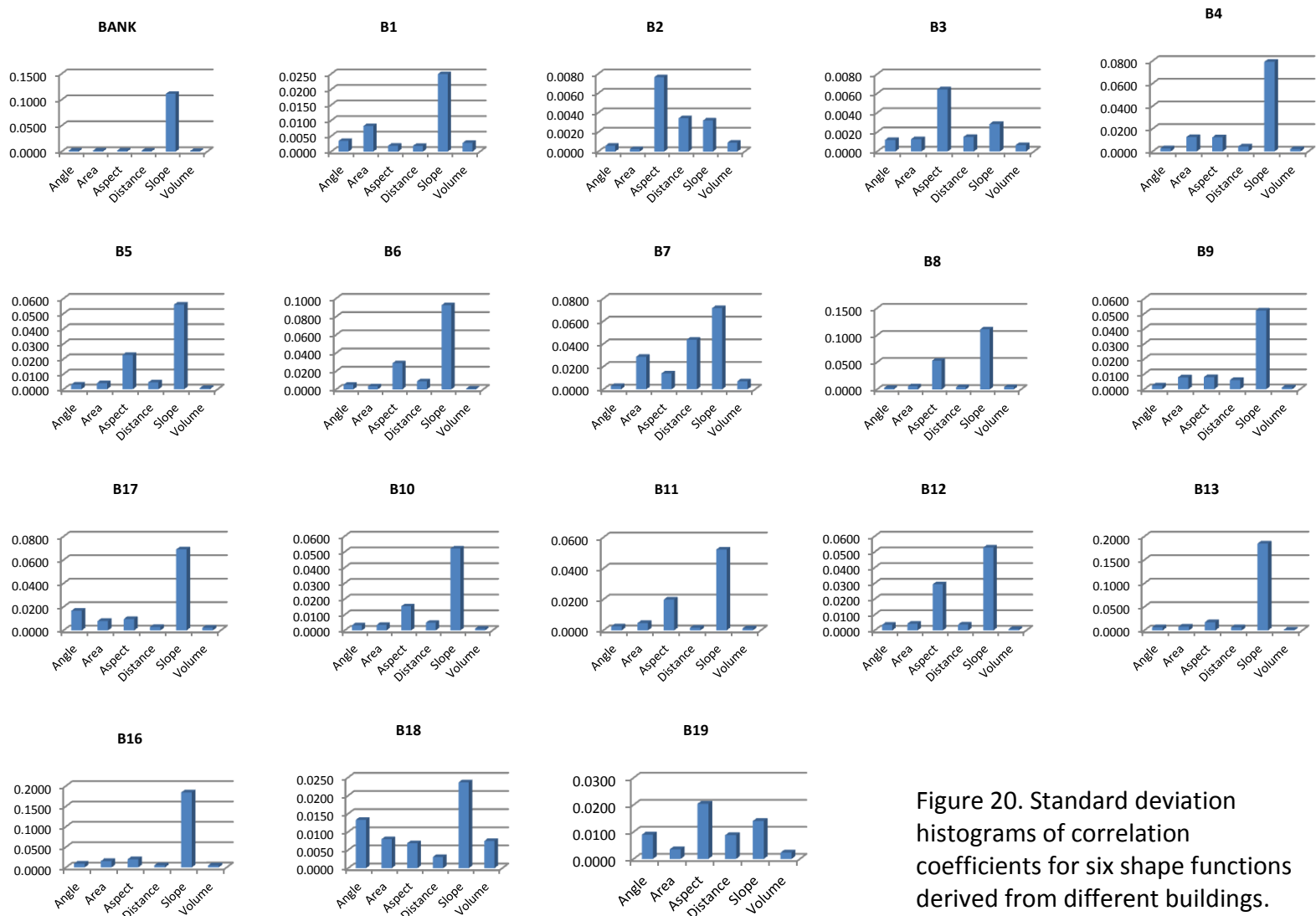


Figure 20. Standard deviation histograms of correlation coefficients for six shape functions derived from different buildings.

Error tolerance

Errors cannot be fully avoided from user-generated 3D building models because influencing factors are multitudinal, such as low acquaintance with location, interfering features on roofs, or complication of buildings. From the “Dissimilarity Analysis” section, it can be seen that the Bank building model has relatively high quality. Here, this building model is used to determine a range of error tolerance. Figure 21 plots the shape distribution of the Bank building with varying heights: -50%, -25%, -20%, -15%, -10%, -5%, 5%, 10%, 15%, 20%, 25%, and 50%.

As shown in Table 9, slope is the most sensitive shape function when the building height increases or decreases by the percentage intervals mentioned above. Even between the LiDAR-derived building model and the original user-generated 3D building model, the correlation coefficient for the slope shape function is only 0.94. In the paper by Dong and Guo (2011), a correlation coefficient of 0.99 is proposed as the threshold for detecting major changes in 3D building shapes. In other words, if the correlation coefficient between two shape functions obtained from a LiDAR-derived building model and a user-generated building model is greater than or equal to 0.99, the LiDAR-derived building model can be considered the same as the user-generated building model. If the LiDAR data is collected in a post-earthquake scenario, then the correlation coefficient threshold 0.99 can be used to detect buildings with major damages. Following this assumption, it can be seen from Table 9 that most shape functions (except slope) can be used to compare LiDAR-derived building models with user-generated building models

for detecting major building damage, even though the height of the user-generated building model is 20% more or less than the actual building height. Beyond the +/-20% range, it would be difficult to tell if the differences in the correlation coefficients are caused by major building damage or inaccurate user-generated building models.

The D_50% curve in each shape function graph is much more distinct from other curves and even the I_50% curve in Figure 21. Since the building loses part of the building structure (Figure 22), the shape distribution of each function has apparent differences from its original model. Meanwhile, the D_50% correlation coefficients of the six functions in Table 4 are much lower than others.

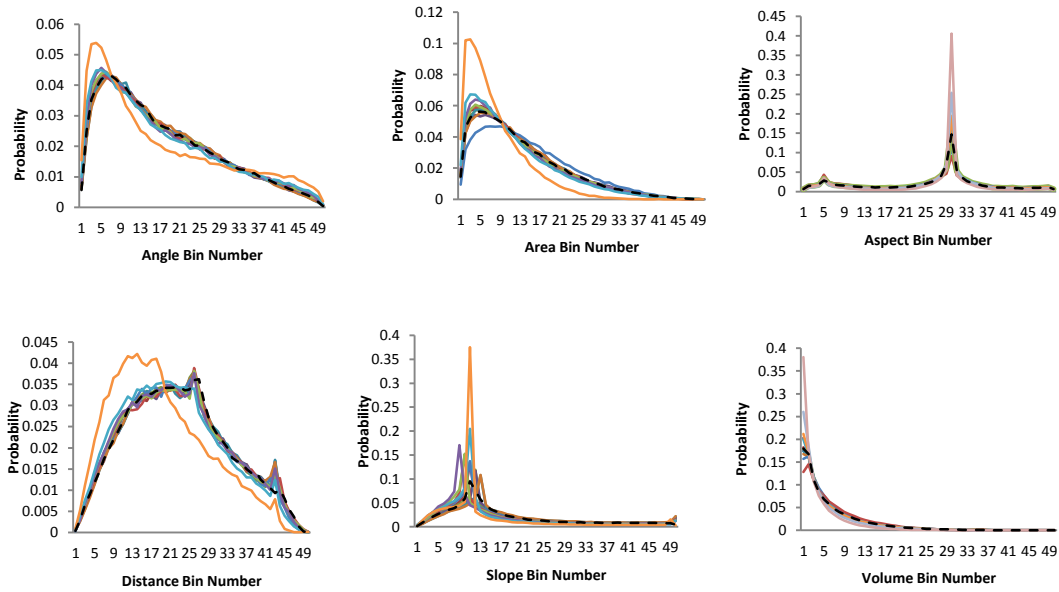


Figure 21. 3D Shape Signatures of six shape functions.

Table 4. Correlation Coefficients between the 3D LiDAR Model and the 3D VGI Model with Different Height Changes.

	Original	I_5%	I_10%	I_15%	I_20%	I_25%	I_50%	D_5%	D_10%	D_15%	D_20%	D_25%	D_50%
Angle	0.9989	0.9985	0.9984	0.9980	0.9974	0.992	0.9739	0.9983	0.9966	0.9956	0.9916	0.9824	0.8801
Area	0.9986	0.9995	0.9988	0.9992	0.9982	0.9967	0.9696	0.9993	0.9977	0.9974	0.9927	0.9840	0.8947
Aspect	0.9919	0.9922	0.9922	0.9930	0.9937	0.9872	0.9612	0.9914	0.9891	0.9894	0.9859	0.9745	0.9219
Distance	0.9935	0.9930	0.9925	0.9919	0.9923	0.9857	0.9752	0.9923	0.9946	0.9934	0.9882	0.9749	0.8162
Slope	0.9428	0.9154	0.9038	0.8508	0.8213	0.9493	0.8792	0.9262	0.7564	0.7170	0.6152	0.8704	0.7067
Volume	0.9998	0.9997	0.9995	0.9992	0.9989	0.9820	0.9820	0.9986	0.9982	0.9979	0.9957	0.9801	0.9118

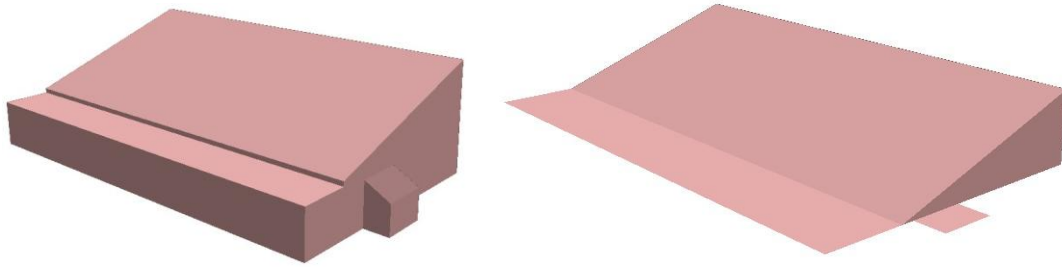


Figure 22. The actual building model and the modified building model with 50% decrease in height.

Special case

In the real world, many buildings have indented vertical walls as shown in Figure 23, or there are even no walls in some structures such as pavilions. Users may prefer to create these 3D models the same as the real structures, as shown in the Multipatch 2 model of a building in Fremont, California (Figure 24). Since LiDAR points may not be collected from the indented vertical walls, direct comparison between shape functions derived from LiDAR data and 3D building models with indented walls may create false alarms which indicate the building is damaged but in fact it is intact. In such cases, “projected building shells” can be generated by projecting the building roof onto the ground to create vertical walls along the roof boundary (Multipatch 1 in Figure 23). Correlation coefficients (r) in Table 5 show that Multipatch 1 is more similar to the 3D LiDAR model than Multipatch 2. For Multipatch 1, except for the aspect function, other correlation coefficients of the five functions are greater than 0.99. However, for

Multipatch 2, all correlation coefficients are less than 0.99, especially the aspect and slope functions which show significant differences compared with Multipatch 1.

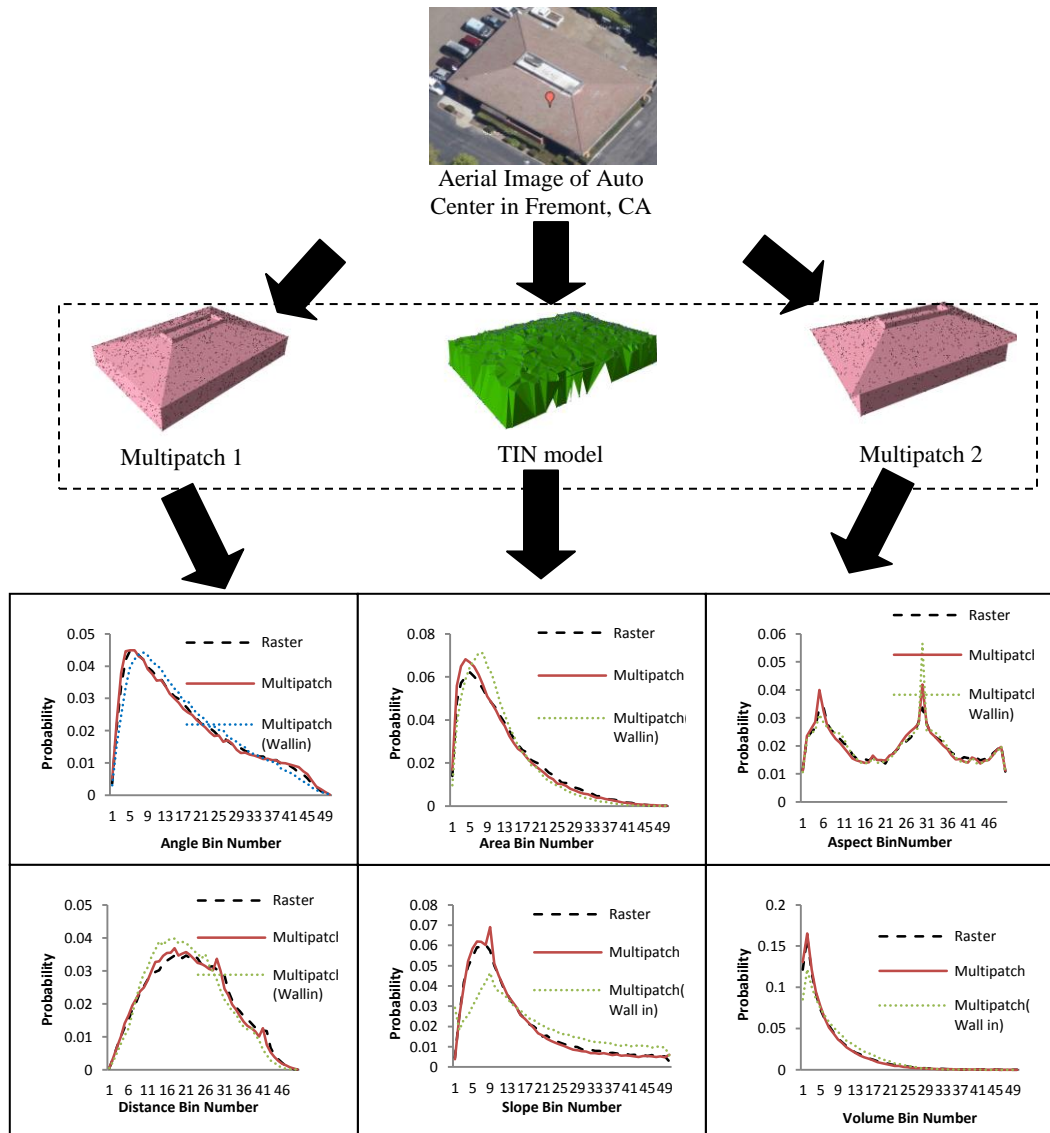


Figure 23. Comparisons of 3D shape signatures for a building derived from LiDAR point clouds and the Google Building Maker.

Table 5. Correlation Coefficients between 3D Shape Signatures (LM1 - LiDAR vs. Multipatch 1, and LM2 - LiDAR vs. Multipatch 2).

	Angle	Area	Aspect	Distance	Slope	Volume
LM1	0.9966	0.9953	0.9700	0.9926	0.9960	0.9994
LM2	0.9800	0.9813	0.8859	0.9736	0.9030	0.9785

CHAPTER 6

DISCUSSION AND CONCLUSION

Volunteered geographic information (VGI), as a new paradigm for geographic information production, allows for public participation in spatial data collection. Major VGI efforts have focused on social media and 2D spatial data collection, and 3D VGI is a new area that needs more investigative efforts. Using Google Building Maker, Internet users can conveniently create 3D building models for many cities and share the models in Google Warehouse. Using 3D modeling tools such as Google Building Maker, grassroots citizens can potentially create 3D urban models in an inexpensive, affordable, and timely manner.

An important application of 3D VGI is for supporting rapid disaster response and damage assessment. 3D building models can be created anytime during the disaster preparation stage or immediately following a disaster, and used as pre-event data. Other geospatial data such as LiDAR data can be collected after the disaster as post-event data. New methods can be developed for rapid comparison of pre-event and post-event data. Such an approach for disaster response and damage assessment can be more effective and efficient because: (1) data analysis can be carried out in an automated way; (2) damage assessment can be conducted at the building scale and

district/regional scale; and (3) disaster mapping, analysis and reporting can be integrated seamlessly.

In the study, user-generated 3D building models from Google Building Maker were compared with LiDAR-derived building models using 3D shape signatures. Eighteen 3D building models were created in Fremont, California using the Google Building Maker, and six shape functions (distance, angle, area, volume, slope, and aspect) were applied to the 18 LiDAR-derived building models and user-generated ones. A special case regarding the comparison between LiDAR data and building models with indented walls was also discussed. Based on the results, the following conclusions are drawn:

- (1) Distance, angle, area, volume and aspect can be used as shape functions for comparison of user-generated building models and LiDAR-derived building models.
- (2) Slope as a shape function is very sensitive to building height variation and should be used with care. When building height is not accurate enough (which is a common problem for user-generated building models), shape signatures calculated from slope can be misleading.
- (3) Most of the six shape functions (except slope) can be used to compare LiDAR-derived building models with user-generated building models for detecting major building damage, even though the height of the user-generated building model is 20% more or less than the actual building height.

However, beyond the +/-20% range, it would be difficult to tell if the differences in the correlation coefficients are caused by major building damage or inaccurate user-generated building models.

- (4) When compared with LiDAR data, 3D building models with indented walls may create false alarms which indicate the building is damaged but in fact it is intact. In such cases, “projected building shells” can be generated by projecting the building roof onto the ground to create vertical walls along the roof boundary, then comparisons can be made between the projected building shells and LiDAR data.
- (5) 3D shape signatures may not detect minor changes in 3D building models. However, this should not be a problem if the 3D shape signatures are used for detecting major changes in building shapes, such as major building damages after a disaster.

There are several limitations of this study that need to be further investigated:

- (1) Since the author is the only data provider for the user-generated building models, more evaluations using 3D building models created by different users are necessary.
- (2) When simulating errors in 3D building models induced by ordinary Internet users, for simplicity only errors in building height are taken into account in

this study. Actual errors in user-generated 3D building models can be more complex, and more advanced simulations may be necessary in the future.

- (3) The behavior of VGI data providers may greatly affect the quality of VGI, and this is a topic beyond the scope of this study. However, how to improve the data quality by providing basic training or tutorials for ordinary VGI providers is an important question that affects the wide application of VGI, including user-generated 3D building models.

REFERENCES:

- Aberley, D. and Sieber, R. (2002). Public Participation GIS (PPGIS) guiding principles. First International PPGIS Conference, URISA, Rutgers University New Brunswick New Jersey July 20–22: URISA.
- Alexander, C., Smith-Voysey, S., Jarvis, C., & Tansey, K. (2009). Integrating building footprints land LiDAR elevation data to classify roof structures and visualize buildings. *Computers, Environment and Urban Systems*, 33, 285-292.
- Armit A. (1971). Multipatch and multiObject design systems. *Proceedings of the Royal Society London*, Vol. A 321, p 235.
- Barnes, S. J. (2003). Location-Based Services. *E-Service Journal*, 2(3), 59-70.
- Bapsavias, E., Mason, S., and Stallmann, D. (1995). Use of DSMs/DSMs and othoimages to support building extraction. *Automatic Extraction of Man-Made Objects from Aerial and Space Images*, 199-210.
- Benner, J., Geiger, A., & Leinemann, K. (2005). Flexible generation of semantic 3d building models. Paper presented at the 1st International Workshop on Next Generation 3D City Models, Bonn, Germany.

- Brenner, A., Zwally, J., Bentley, C., Csatho, B., Harding, D., Hofton, M., Minster, B., Roberts, L., Saba, J., Thomas, R., Yi, D. (2003). Geoscience laser altimeter system (GLAS) - derivation of range and range distributions from laser pulse waveform analysis for surface elevations, roughness, slope, and vegetation heights. Algorithm Theoretical Basis Document - Version 4.1.
- Bugs, G., Granell, C., Fonts, O., Huerta, J., & Painho, M. (2010). An assessment of public participation GIS and Web 2.0 technologies in urban planning practice in Ganela, Brazil. *Cities*, 27, 172-181.
- Charalambos Poullis, S. Y. and Neumann, U. (2008) Rapid creation of large scale photorealistic virtual environments. *VR*, pp. 153–160.
- Coleman, D. J. and Eng, P. (2010) Volunteered geographic information in spatial infrastructure: An early look at opportunities and constraints. GSDI 12 WORLD CONFERENCE.
- Coleman, D.J., Sabone, B. and Nkhwanana, N. (2010). Volunteering Geographic Information to Authoritative Databases: Linking Contributor Motivations to Program Effectiveness. *Geomatica*, 64(1), 383-396.
- COLLADA, (2007). Message posted to <https://collada.org/mediawiki/index.php/COLLADA>.

- Dong, P. and Guo, H. (2011). A framework for automated assessment of post-earthquake building damage using geospatial data. *International Journal of Remote Sensing*, 1-20.
- Elmadhoun, A. M. A. (2010). Using neogeography technology to support participatory spatial planning. International Institute For Geo-Information Science And Earth Observation Enschede, The Netherlands.
- ESRI (2011,September 20) Message posted to <http://www.esri.com/news/arcwatch/0311/power-of-vgi.html>.
- Frueh, C., Sammon, R. and Zakhor, A. (2004). Automated texture mapping of 3d city models with oblique aerial imagery. In: Proceedings of 2nd International Symposium on 3D Data Processing, Visualization and Transmission, Thessaloniki, Greece, 396-403.
- Früh, C., Sammon, R., and Zakhor, A. (2004). Automated texture mapping of 3d city models with oblique aerial imagery. *3D Data Processing, Visualization and Transmission*, 396 – 403.
- Früh, C. and Zakhor, A. (2004). An automated method for large-scale, groundbased city model acquisition. *Int. J. Comput*, 60, pp. 5–24.
- Goetz, M. & Zipf, A. (2011). Towards defining a framework for the automatic derivation of 3D CityGML models from volunteered geographic information. Joint ISPRS

Workshop on 3D City Modelling & Applications and the 6th 3D GeoInfo Conference. Wuhan, China.

Goodchild, M. J. (2007a). Citizens as sensors: the world of volunteered geography. *GeoJournal*, 69 (4), 211-221.

Goodchild, M. J. (2007b). Citizens as voluntary sensors: Spatial data infrastructures in the world of Web 2.0. *International Journal of Spatial Data Infrastructure Research*, 2, 24-32.

Goodchild, M. F., Fu, P., and Rich, P. (2007). Sharing geographic information: An assessment of the geospatial onestop. *Annals of the Association of American Geographers*, 97(2), 249–265.

Goodchild, M. F. and Glennon, J. A. (2010). Crowdsourcing geographic information for disaster response: a research frontier. *International Journal of Digital Earth*, 3 (3), 231-241.

Google Building Maker (2009). Message posted to <http://blogscoped.com/archive/2009-10-14-n18.html>

Google Earth (2012). Message posted to <http://www.google.com/earth/index.html>

Google SketchUp Blog, (2009). message posted to <http://sketchupdate.blogspot.com/2009/03/new-file-format-for-models-in-3d.html>.

- Gould, M. (2007). Vertically interoperable geo-infrastructures and scalability. Specialist Meeting on Volunteered Geographic Information. Santa Barbara Conference.
- Gröger, G., Kolbe, T. H., Czerwinski, A., & Nagel, C. (2008). OpenGIS city geography markup language (CITYGML) encoding standard – Version 1.0.0. OGC Doc, No. 08-007r1.
- Guo, H. D., Liu, Z., and Zhu, L. W. (2010). Digital Earth: decadal experiences and some thoughts. *International Journal of Digital Earth*, 3 (1), 31-46.
- Haala, N., Brenner, C. (2001). City model data acquisition from laser scanning. On OEEPE/ISPRS-workshop 'From 2D to 3D – Establishment and Maintenance of National Core Geospatial Databases, Hannover.
- Haala, N., and Hahn, M. (1995). Data fusion for the detection and reconstruction of buildings. In Automatic Extraction of Man-Made Objects from Aerial and Space Images (pp. 211–220).
- Haklay, M., Singleton, A, and Parker, C. (2008). Web mapping 2.0: the neogeography of the geoweb. *Journal Compilation*, 2011-2039.
- Huertas A., Nevatia R. (1988). Detecting buildings in aerial images. *Computer Vision, Graphics and Image Processing*, 41(2), 131-152.
- Hudson-Smith, A. and Evans, S. (2003). Virtual cities: From CAD to 3D GIS. Advanced Spatial Analysis: *The CASA book of GIS*, P41-60.

- Jones, K. (2011). Communicating perceived geospatial data quality of 3d objects in virtual globes. Memorial University of Newfoundland. Retrieved from http://yvanbedard.scg.ulaval.ca/wp-content/documents/these/Memoire_KristaJones.pdf
- Kolbe, T. H., Gröger, G., & Plümer, L. (2005). CityGML – interoperable access to 3d city models. Paper Presented at the 1st International Symposium On Geo-Information for Disaster Management, Delft, Netherlands.
- Kolbe, H.T., Plümer, L., & Cremers, A.B. (2000). Identifying buildings in aerial images using constraint relaxation and variable elimination. *IEEE Intell.Syst.Appl*, 15(1), 33-39.
- Lari, Z. & Ebadi, H. (2004). Automatic extraction of building features from high resolution satellite images using artificial neural network. Proceeding of ISPRS Conference on Information Extracting from SAR and Optical Data with Emphasis on Developing Countries, Istanbul, Turkey.
- Lathrop, R. G., Montesano, P., Tesauro, J., and Zarate, B. (2005). Statewide mapping and assessment of vernal pool: A New Jersey case study. *Journal of Environmental Management*, 76, 230–238.

- Li, M. C., Cheng, L., Gong, J. Y., Liu Y. X., Chen, Z. J., Li, F. X., Chen, G., Chen, D., & Song, X. G. (2008). Post-earthquake assessment of building damage degree using LiDAR data and imagery. *Sci China Ser E-Tech Sci*, 51, 133-143.
- Liu, W., Dong, P., Liu, J.B., and Guo, H.D., (2012). Evaluation of three-dimensional shape signatures for automated assessment of post-earthquake building damage. *Earthquake Spectra*. (in press).
- National Research Council. (2007). Successful response starts with a map: improving geospatial support for disaster management. Washington: National Academies Press. Retrieved from http://dels.nas.edu/resources/static-assets/materials-based-on-reports/reports-in-brief/successful_response_final.pdf.
- Neubauer, N., Over, M., and Zipf, A. (2008). Virtual Cities 2.0: generating web-based 3D city models and landscapes based on free and user generated data (OpenStreetMap). Retrieved from <http://www.geographie.uni-bonn.de/karto/>.
- Over, M., Schilling, A., Neubauer, S., and Zipf, A. (2010). Generating Web-based 3D city models form OpenStreetMap: The current situation in Germany. *Computers, Environment, and Urban System*, 5(1).
- Pollefeys, M., Nist'er, D., Frahm, J. M., Akbarzadeh, A., Mordohai, P., Clipp, B., Engels, C., Gallup, D., Kim, S. J., Merrell, P., Salmi, C., Sinha, S., Talton, B., Wang, L., Yang, Q.,

- Stew'enius, H., Yang, R., Welch, G., and Towles, H. (2008). Detailed real-time urban 3D reconstruction from video. *Int. J. Comput. Vision*, vol. 78, pp. 143–167.
- Sabone, B. (2009). Assessing alternative technologies for use of volunteered geographic information in authoritative databases. Department of Geodesy and Geomatics Engineering University of New Brunswick. Retrieved from <http://gge.unb.ca/Pubs/TR269.pdf>
- Sahar, L. & Krupnlk, A. (1999). Semiautomatic extraction of building outlines from large-scale aerial images. *Photogramm. Eng. Remote Sens.*, 65(4), 459-465.
- Sahar, L., Muthukumar, S., & French, S.P. (2010). Using aerial imagery and GIS in Automated building footprint extraction and shape recognition for earthquake risk assessment of urban inventories. *IEEE Transactions on Geoscience and Remote Sencing*, 48(9), 3511-3520.
- Schilling, A., Over, M., Neubauer, S., Neis, P., Walenciak, G., & Zipf, A. (2009). Interoperable location based services for 3d cities on the web using user generated content from OpenStreetMap. Paper presented at the 27th Urban Data Management Symposium (UDMS 2009), Ljubljana , Slovenia.
- Seeger, C. (2008). The role of facilitated volunteered geographic information in the landscape planning and site design process. *GeoJournal*, 72 (3), 199-213.

Sheppard, S. R. J. and Cizek, P. (2009). The ethics of Google Earth: crossing thresholds from spatial data to landscape visualization. *Journal of Environmental Management*, 90 (6), 2102-2117.

SketchUp, (2012). Retrieved January 31st, 2012 from

<http://support.google.com/sketchup/bin/answer.py?hl=en&answer=1004163>

Song, W., & Sun, G. (2010). The role of mobile volunteered geographic information in urban management. Paper presented at the 18th International Conference on Geoinformatics, Beijing, China, 1 – 5.

The Essentials of a TIN model. (n.d.). Retrieved January 30th, 2012 from

http://planet.botany.uwc.ac.za/nisl/GIS/spatial/chap_1_50.htm.

TomTom (2007). Get to know TomTom MapShare. Message posted to

<http://www.clubtomtom.com/general/get-to-know-tomtom-mapshare%E2%84%A2/>.

TomTom (2009). TomTom Investor Relations Company Profile. Message posted to

<http://investors.tomtom.com/overview.cfm>

Tse, O.C.R., Gold, C. and Kidner, D. (2004). An original way of building a tin with complex urban structures. *In Proceedings of ISPRS*, 931-936.

Tulloch, D. (2008). Is VGI participation? From vernal pools to video games. *GeoJournal* 72(3):161-171.

Turner, J. A., (2006). Introduction to neogeography. O'Reilly Media.

Turner, J. A., (2010). OpenStreetMap Haiti. Message posted to

<http://opensource.com/life/10/1/openstreetmap-haiti>.

Wang, O., Lodha, S.K., & Helmbold, D.P. (2006). A bayesian approach to building footprint extraction from aerial lidar data. *In 3DPVT'06*, 192–199.

Wei, Y., Zhao, Z., and Song, J. (2004). Urban building extraction from high-resolution satellite panchromatic image using clustering and edge detection. *IEEE Proceeding of IGARSS*, 3, 2008-2010.

Xiao, Y. , Lim, S.K. , Tan, T.S. , & Tay, S.C. (2004). Feature extraction using very high resolution satellite imagery. *Geoscience and Remote Sensing*, 3, 2004-2007.

Zhou, G., Song, J., Simmers, J., & Cheng, P. (2004). Urban 3D GIS from LiDAR and digital aerial images. *Computers & Geosciences*, 30, 345-353.